Metabolic characterisation of transglutaminase 2 inhibitor effects in breast cancer cell lines

Mariana Gallo[1] (iD), Elena Ferrari[1], Anna Terrazzan[2], Federica Brugnoli[2], Alberto Spisni[1] (iD), Cristian Taccioli[3], Gianluca Aguiari[4], Alessandro Trentini[5], Stefano Volinia[2], Jeffrey W. Keillor[6], Carlo M. Bergamini[4], Nicoletta Bianchi[2] (iD) and Thelma A. Pertinhez[1]

1 Department of Medicine and Surgery, University of Parma, Italy
2 Department of Translational Medicine, University of Ferrara, Italy
3 Department of Animal Medicine, Production and Health (MAPS), University of Padua, Italy
4 Department of Neuroscience and Rehabilitation, University of Ferrara, Italy
5 Department of Environmental Sciences and Prevention, University of Ferrara, Italy
6 Department of Chemistry and Biomolecular Sciences, University of Ottawa, Canada

Transglutaminase 2 (TG2), which mediates post-translational modifications of multiple intracellular enzymes, is involved in the pathogenesis and progression of cancer. We used ^{1}H-NMR metabolomics to study the effects of AA9, a novel TG2 inhibitor, on two breast cancer cell lines with distinct phenotypes, MCF-7 and MDA-MB-231. AA9 can promote apoptosis in both cell lines, but it is particularly effective in MD-MB-231, inhibiting transamidation reactions and decreasing cell migration and invasiveness. This metabolomics study provides evidence of a major effect of AA9 on MDA-MB-231 cells, impacting glutamate and aspartate metabolism, rather than on MCF-7 cells, characterised by choline and O-phosphocholine decrease. Interestingly, AA9 treatment induces myo-inositol alteration in both cell lines, indicating action on phosphatidylinositol metabolism, likely modulated by the G protein activity of TG2 on phospholipase C. Considering the metabolic deregulations that characterise various breast cancer subtypes, the existence of a metabolic pathway affected by AA9 further points to TG2 as a promising hot spot. The metabolomics approach provides a powerful tool to monitor the effectiveness of inhibitors and better understand the role of TG2 in cancer.

Introduction

The present study focuses on the emerging relevance of Transglutaminase 2 (TG2) in breast cancer (BrCa) [1]. This enzyme plays a role in inflammation [2–4], mediates the onset of drug resistance [5–7], and controls epithelial-to-mesenchymal transition (EMT), sustaining the motility and invasiveness of BrCa cells [8–10]. However, how TG2 intervenes in these pathological processes is complex, depending primarily on its dual action, derived from its ability to act both as a G protein and to catalyse transamidation reactions [11]. It has been suggested that GTP-binding function may be associated with EMT [12] and with processes linked to metastatic features of BrCa cells, such as activation of the autophagosome [13]. At the same time,

Abbreviations

BAP, N-(5-Aminopentyl)biotinamide trifluoroacetate salt; BrCa, breast cancer; EMT, epithelial-to-mesenchymal transition; FDR, false discovery rate; GAPDH, Glyceraldehyde-3-phosphate dehydrogenase; NMR, nuclear magnetic resonance; PBS, phosphate buffered saline; RT-qPCR, reverse transcription and quantitative polymerase chain reaction; Pgp (or ABCB1), P-glycoprotein 1; PLA2, phospholipase A2; PLC-δ1, phospholipase C-δ1; PLS-DA, partial least squares-discriminant analysis; TG2, transglutaminase 2; VIP, variable importance in projection.

transamidation activity correlates somewhat with drug resistance [14] and influences the formation of metastatic niches [15]. Proteins containing surface-exposed glutamine residues are suitable for cross-linking reactions with primary amines (lysine residues or polyamines) and are potential targets of TG2-catalysed transamidation reactions. Glyceraldehyde-3-phosphate dehydrogenase (GAPDH) and α-ketoglutarate dehydrogenase [16,17], and other enzymes, for example, aldolase, fatty acid synthase, and cytochrome c have been identified as *in vitro* TG2 targets [18]. It is a prevalent opinion that TG2 mediates the inactivation of its targets, although its action on phospholipase A2 (PLA2) leads to increased activity of the enzyme and thus to a higher production of eicosanoids during the inflammatory process [19,20]. Furthermore, the interaction between phospholipase C-δ1 (PLC-δ1) and TG2, acting as a G protein, blocks the downstream signalling pathway [21]. This evidence suggests that TG2 inhibition may have consequences on cellular metabolism, although no functional investigations have been performed, yet, to identify metabolic alterations triggered by TG2.

These features make TG2 a potential target for anticancer drugs [22–25]. A promising TG2 inhibitor is NC9, already tested in several cancer models [10,26–29] and exhibiting a significant apoptotic action against various BrCa cell lines, especially in combination with standard drugs [26]. Figure 1 depicts the chemical structures of NC9 and its more potent derivative, AA9. The acrylamide group is the most commonly used functional group in the resurgent field of targeted covalent inhibitors, by virtue of its inherent aqueous stability and limited off-target reactivity that enable effective design [30]. Indeed, judiciously designed TG2 inhibitors bearing an acrylamide warhead react nearly one billion-fold more rapidly with their target than with adventitious thiols, which greatly reduces the chance of off-target effects [31]. In AA9, the C-terminal dansyl group of NC9 is replaced by a naphthyl moiety, and the long, flexible polyethylene glycol linker of NC9 is substituted by a rigid piperazine core [32]. This structural layout improves the AA9 inhibitory efficacy, resulting in greater selectivity and effectiveness on TG2 transamidation and GTP-binding activities than NC9 [32–34].

While large-scale proteomic studies report the consequences of genetic and environmental modifications, metabolomics extensively describes the molecules generated by native or modified enzymes and pathways [35–37].

Metabolic reprogramming is a hallmark of cancer cells, as it sustains their development and survival/resistance under stressful conditions [38,39]. Identifying

metabolic alterations is expected to offer insights into the disease's molecular mechanisms and possible new targets for therapy. In this context, we analysed the impact of the TG2 inhibitors NC9 and AA9 on two BrCa cell lines, the hormone-sensitive MCF-7 and the hormone-independent MDA-MB-231, the latter characterised by a more aggressive phenotype and a higher level of TG2 expression [26]. Previous metabolomic studies on these cell lines revealed changes in the concentration of many metabolites after exposure to several drugs or other treatments [40–48].

We first investigated the membrane permeability properties of AA9 in comparison with the parent compound NC9 and some functional features: their capability to inhibit *in situ* TGase activity and their effect on motility, invasion, and apoptosis. Finally, we employed ^{1}H-nuclear magnetic resonance (^{1}H-NMR) spectroscopy to investigate the effects of AA9 treatment on the metabolic profiles of BrCa cell lines. The results have been analysed and correlated to specific genomic features of the two cell lines with the aim to find metabolic hot spots for novel anticancer molecules [49–51].

Results

Membrane permeability assay of AA9

As cellular compartmentation is a critical parameter in the evaluation of drug efficacy, we have estimated membrane permeability through an artificial lipid membrane and cellular membranes. We measured AA9 passive diffusion using a parallel artificial membrane permeability assay (PAMPA) and obtained the value of $P_e = 10.5 \times 10^{-6}$ cm·s^{-1}, where P_e is the effective permeability coefficient. This value indicates good passive permeability.

For the diffusion through a cell layer, we used Madin-Darby canine kidney cells, transfected to express the efflux transporter P-glycoprotein 1 (Pgp/ABCB1, an ABC exporter).

To better understand the pharmaceutical relevance of these measurements, we compared AA9 to NC9. AA9 is over 10 times more cell-permeable than NC9, with P_{app} (A → B) = 0.84×10^{-6} cm·s^{-1} in the apical to basolateral direction and P_{app} (B → A) = 21.55×10^{-6} cm·s^{-1} in the basolateral to apical direction. Consequently, AA9 shows a better efflux ratio of 25.8, nearly 10 times lower than the value of 224 measured for NC9.

Since ABC transporters such as Pgp mediate multidrug resistance to several anti-cancer agents, as in the case of doxorubicin [52], we verified their possible
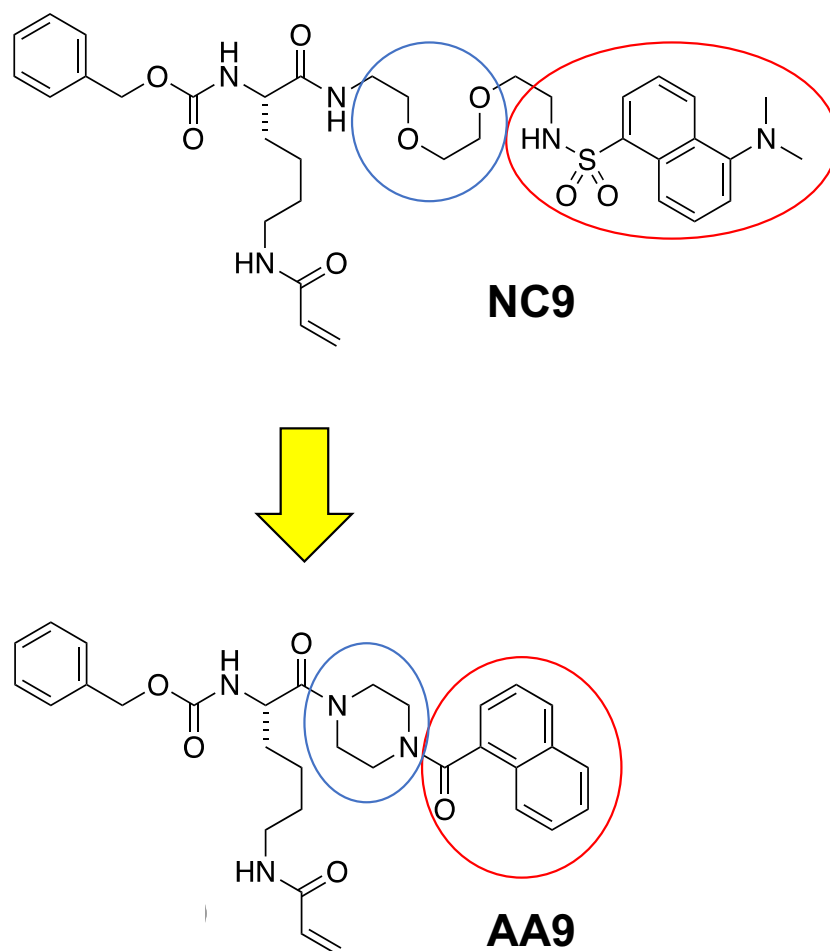
Fig. 1. Chemical structure of the TG2 inhibitors employed in the study. The C-terminal dansyl group (circled in red) and the polyethylene glycol linker (circled in blue) of NC9 have been replaced by naphthyl moiety and the rigid piperazine core in AA9.

interference by analysing AA9 permeability and efflux ratios upon Pgp inhibition. In the presence of 10 μM Zosuquidar, a known Pgp inhibitor [53], we measured an increase in apical to basolateral permeability, P_{app} $(A \rightarrow B) = 9.58 \times 10^{-6}$ cm·s^{-1}, and a decrease in basolateral to apical diffusion, P_{app} $(B \rightarrow A) = 9.94 \times 10^{-6}$ cm·s^{-1}, giving an efflux ratio of 1.04, thus highlighting the expected intervention of the Pgp transporter.

Transamidase activity decreased by AA9 in BrCa cells

We analysed *in situ* TG2 transamidation activity [54] in live BrCa cells untreated and treated for 1 h with the inhibitors, evidencing a strong decrease only in the MDA-MB-231 exposed to AA9 (Fig. 2A, red columns). This assay is detailed in the Materials and methods section. We underline that these cells express

higher TG2 mRNA levels than MCF-7 cells, as appreciable in Fig. 2B and quantified by reverse transcription and quantitative polymerase chain reaction (RT-qPCR).

Also, to assay the effects on MCF-7 cells, we developed an *in vitro* test aimed at (a) allowing the detection of transamidase activity and (b) eliminating any bias due to the possible low permeability of the cell membrane. Thus, we used t75 flasks instead of t25 flasks for culturing cells (untreated or treated for 1 h with the selected compounds). After incubation, we collected and lysed the cells, and subsequently, we performed the assay for catalytical activity. The results demonstrated a residual transamidase activity of about 75% in the cells treated with both AA9 and NC9 (Fig. 2A, blue columns). We further carried out experiments in which we directly exposed the cellular lysates of MDA-MB-231 and MCF-7 to 10 μM of AA9, resulting in a decrease of the *in vitro* transamidase
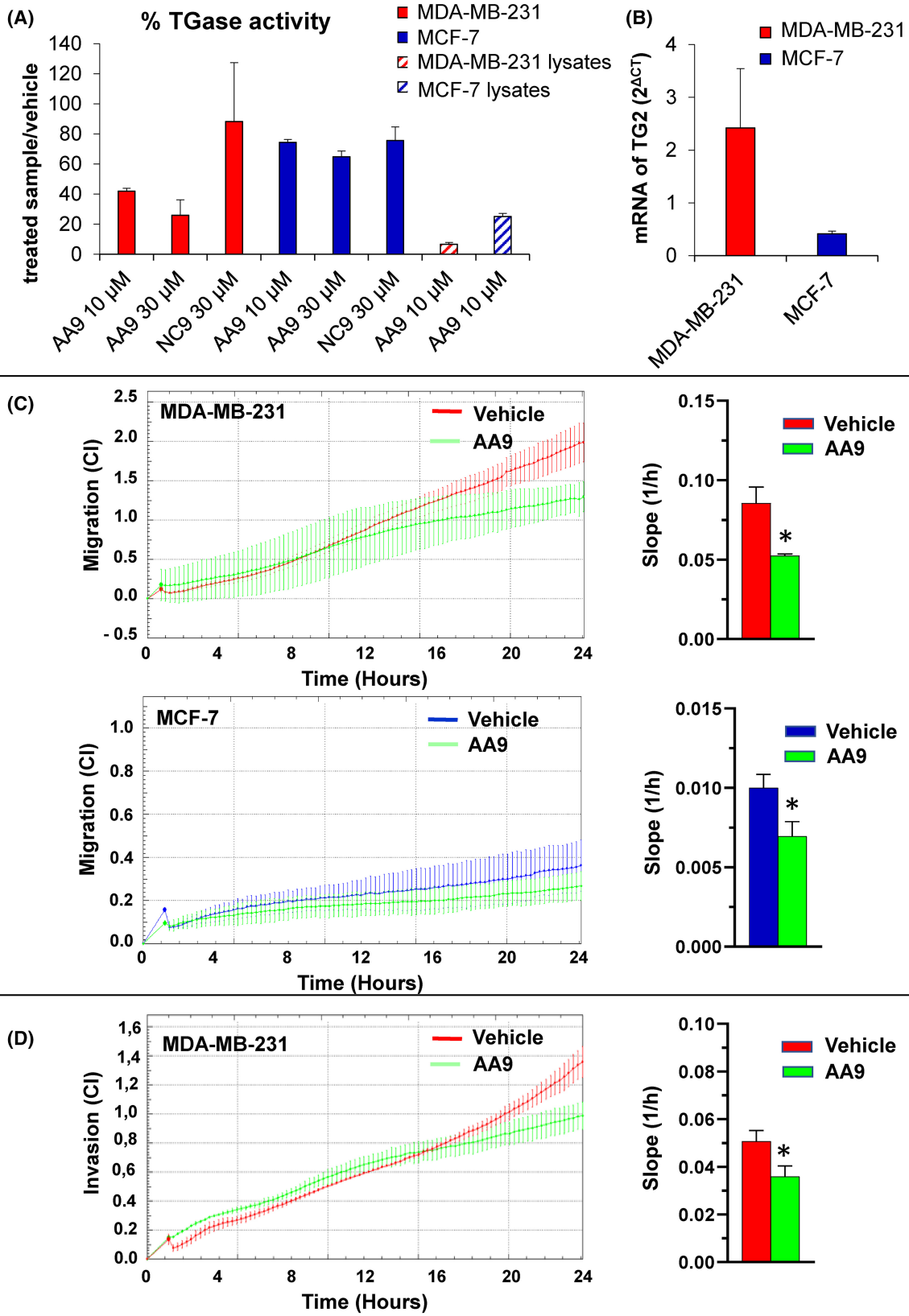
Fig. 2. Inhibition of transamidase activity, TG2 expression, and effects of inhibitors on cell motility in BrCa cells. (A) Red columns, *in situ* assay, in which has been tested the transamidase activity of MDA-MB-231 cells treated with the compounds and then exposed to BAP and ionophore solution to stimulate *in vivo* catalysis; blue columns, *in vitro* assay of the MCF-7 cells treated with the compounds and subsequently exposed to BAP to carry out transamidation reactions; hatched columns, *in vitro* test of MDA-MB-231 (red lines) and MCF-7 (blue lines) lysates collected and then incubated with 10 μM AA9. The percentage of transamidase activity inhibition was determined by comparing the value detected in the treated samples to the control supplemented only with vehicle (0.1% DMSO) and BAP. Data obtained by triplicate determinations in two independent experiments. (B) Levels of mRNA for TG2 evaluated by RT-qPCR. In red, the results obtained in MDA-MB-231 and in blue in MCF-7 cells. The quantification was done by the geometric mean of two references, as described in Materials and methods, carried out in three independent experiments. AA9 effect on migration (C) and invasion (D). In green, samples treated with AA9, in red or blue, samples were treated only with vehicle of MDA-MB-231 or MCF-7 cells, respectively. On the left, cell dynamic monitoring for 24 h. On the right, CI (cell index) ± SD corresponds to slope analysis, describing the steepness, inclination, gradient, and changing rate of the CI curves over time. All the results were represented as average ± SD of three independent experiments. The statistical analysis reported in the slope histogram was performed by a two-tailed Student's *t* test for unpaired data using the GRAPHPAD PRISM 6.0 statistical package (GraphPad Software, San Diego, CA, USA). We considered *P* values < 0.05 to be statistically significant (*).

activity with a residual value of 6.55% ± 1.22 in MDA-MB-231 (Fig. 2A, red hatched column) and of 25.03% ± 2.14 in MCF-7 cells (Fig. 2A, blue hatched column).

Effects of AA9 on the motility and invasion of BrCa cells

The ability of NC9 inhibitors to decrease the motility of BrCa cells has already been demonstrated [10], affecting migration both in MDA-MB-231 and MCF-7 cells, although the latter are less inclined to move. Therefore, we investigated the effects of AA9 at 25 μM on the migration of these cell lines (Fig. 2C). The dynamic migration monitoring shows a decrease in MDA-MB-231 of about 50% compared to the 25% recorded in the MCF-7 cells.

Cell invasion capability, or the ability to overcome a resistance barrier, was measured in a similar test using a Matrigel solution. We monitored only MDA-MB-231, since MCF-7 cells do not have this trait unless adequately stimulated [10]. During a 24 h treatment with AA9, the invasiveness of MDA-MB-231 cells decreased significantly (Fig. 2D).

Apoptotic effects of AA9 and NC9

It is well recognised that, in specific contexts, TG2 plays an anti-apoptotic role [55,56], suggesting that its inhibition may offer a novel strategy for anticancer therapy. Therefore, before investigating the impact of AA9 on cellular metabolism, we compared the pro-apoptotic efficacy of AA9 with respect to NC9.

Table 1 summarises the percentage of apoptotic cells induced by the two TG2 inhibitors. At the employed concentrations (25, 50, and 75 μM), the pro-apoptotic effect ranges between 20% and 35% for both molecules. These compounds had comparable efficacy, showing a similar pro-apoptotic and dose-dependent effect of AA9 and NC9 on MCF-7 cells. The maximal efficacy of AA9 (≈ 30%) is already observed at the lowest tested concentration (25 μM), in MDA-MB-231 cells, suggesting some sort of saturation.

It should be borne in mind that, even if this pro-apoptotic effect is moderate, the interest in TG2 inhibitors is mainly due to their potential use in combination with other chemotherapeutic agents [23,26].

¹H-NMR-based metabolic profiling and multivariate statistical analysis

Considering our data on AA9 membrane permeability, its ability to block TG2 activity, and its effect on migration and invasion properties, we investigated its influence on the metabolome of the two cell lines. We carried out cultures and treatments incubating the cells for 16 h [10,26] with 9 μM AA9 (corresponding to its K_I value [57]) or with 0.1% DMSO as a control. The described experimental conditions allowed the acquisition of high-quality NMR spectra, identifying and quantifying 54 and 47 metabolites in lysates from MCF-7 and MDA-MB-231 cells, respectively. The metabolites were classified into the following categories: amino acids and derivatives, intermediates of central carbon metabolism, carbohydrates and derivatives, lipid-related compounds, nitrogen bases, and other compounds (Fig. 3). Many metabolites presented very different concentrations in the two cell lines, with some differences ranging around one order of magnitude (12% of metabolites). Other metabolites were detected exclusively in one cell line: β-alanine, cis-aconitate, and adenosine were

Table 1. Apoptosis evaluated in MCF-7 and MDA-MB-231 cells after 48 h treatment with NC9 and AA9. The percentage of apoptotic cells reported is the average ± SD of three independent experiments.

	DMSO 0.1%	NC9			AA9		
		25 μM	50 μM	75 μM	25 μM	50 μM	75 μM
MCF-7	18.12 ± 3.50	23.70 ± 2.76	25.08 ± 3.38	35.52 ± 5.05	25.87 ± 1.55	33.03 ± 0.78	36.87 ± 0.68
MDA-MB-231	16.17 ± 1.11	17.02 ± 4.47	24.28 ± 1.13	24.28 ± 1.48	30.67 ± 1.67	26.25 ± 0.36	28.90 ± 1.88

present in MDA-MB-231, whereas glutamine, serine, cystathionine, pyruvate, *O*-phosphoethanolamine, adenine, cytidine, xanthine, and pantothenate were detected in MCF-7 cells.

The heatmap (Fig. 4) shows four well-defined groups correlating with cell lines and treatment. The colour pattern within each group indicates high homogeneity, underlining the method's reproducibility. The dendrogram separates the data of the two cell lines (first branching) and the data grouped by type of treatment (second branching). Overall, the results reflect the differences in metabolome composition of the two BrCa cell lines and highlight the minor impact of AA9 on the MCF-7 metabolic profile.

Figure 5 shows the PLS-DA (Partial Least Squares-Discriminant Analysis) and VIP (Variable Importance in Projection) score plots obtained by using the metabolite concentrations measured with and without AA9 treatment. The PLS-DA (Fig. 5A,B) shows a net response to the treatment with the AA9 inhibitor for both cell lines, as indicated by component 1, which accounts for > 50% of the clusters' separation. The VIP score plot (Fig. 5C,D) illustrates the top 15 metabolites responsible for the PLS-DA clusters' separation, identifying the representative indicators of cells' response to AA9. As can be appreciated, the set of metabolites with VIP scores > 1.3 differs between the two cell lines: in MCF-7, there are alanine, lactate, UDP-N-acetylglucosamine, myo-inositol, pyroglutamate, and cystathionine; in MDA-MB-231, we find hypoxanthine, taurine, creatine, glutamate, proline, choline, malate, NAD$^+$, *sn*-glycero-3-phosphate, inosine, aspartate, and glycine.

Perturbations in metabolic pathways triggered by AA9 in MCF-7 cells

Using the complete ensemble of the measured metabolites in MCF-7 cells, we performed a pathway topological analysis (Fig. 6A). Seven significantly dysregulated pathways ($P < 0.01$ and pathway impact > 0.1) were highlighted (Fig. 6B), and among them, it is worth mentioning the ascorbate and aldarate metabolism that has a high statistical significance ($-\log(P) = 3.02$), a high pathway impact (0.5), and a low false discovery rate (FDR = 0.015) reflecting the significant alteration of myo-inositol (VIP > 1.3), Fig. 5C.

Aiming to identify metabolites with the potential of being unique reporters of TG2 inhibitor action, we included the fold change to generate the volcano plot shown in Fig. 7A (|FC| > 1.5, $P < 0.05$). The box plots in Fig. 7B present the six metabolites with a concentration variation that satisfies the imposed limits upon exposure to the inhibitor.

Out of the six metabolites that undergo the largest concentration change, only choline and *O*-phosphocholine are present in one of the most affected metabolic pathways (Fig. 6B), the glycerophospholipid metabolism, with good statistical significance ($-\log(P) = 2.09$), a good FDR = 0.046, and a high pathway impact (0.11). Recognising that phospholipid metabolism is strongly associated with oncogenesis, the decreased levels of choline and *O*-phosphocholine are expected to impact membrane turnover [58].

A more extensive analysis of the data reveals that AA9 causes a decrease in the levels of alanine (alanine, aspartate, and glutamate metabolism), serine (glycine, serine, and threonine metabolism), and pantothenate (pantothenate and CoA biosynthesis). The reduction of pantothenate can affect many relevant degradative and biosynthetic pathways. Serine biosynthesis supports BrCa cell growth. Thus, its reduced concentration could limit the proliferation rate [59].

Finally, the volcano plot shown in Fig. 7A points to an increase in the pyroglutamate level that could reflect either a mitochondrial metabolic alteration of glutamine or glutamate cyclisation. However, because

Fig. 3. Intracellular metabolite profiles of MCF-7 and MDA-MB-231 control cells. Metabolites of MDA-MB-231 (blue) and MCF-7 cells (light blue) have been class gathered. Data are reported as average concentrations (μM) ± SD, normalised against the protein content (mg), measured in three independent experiments. O-PC, *O*-phosphocholine; O-PEA, *O*-phosphoethanolamine; *sn*-GPC, *sn*-glycerophosphocholine; UDP-glc, uridine diphosphate-glucose; UDP-NAG, uridine diphosphate-*N*-acetylglucosamine.
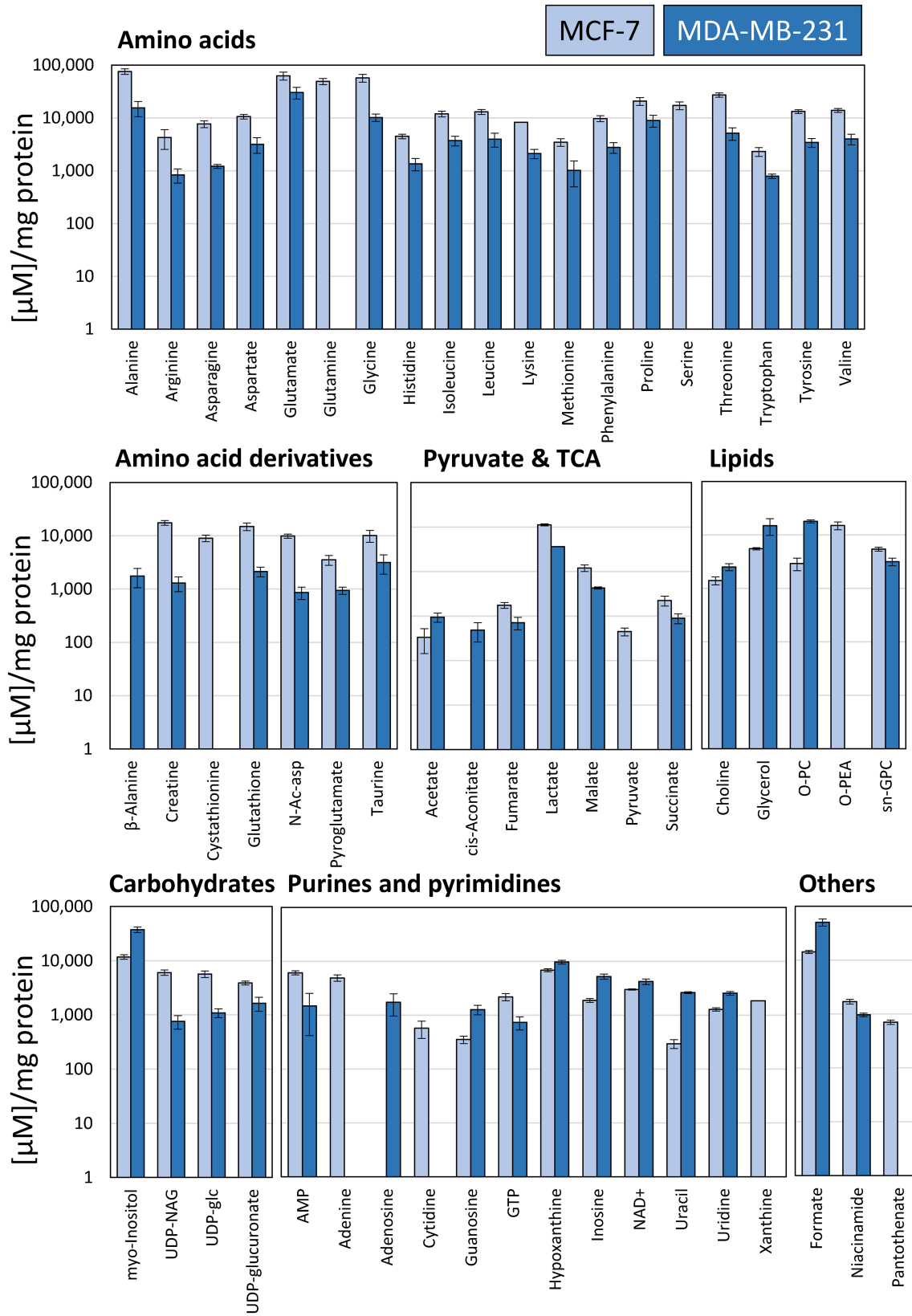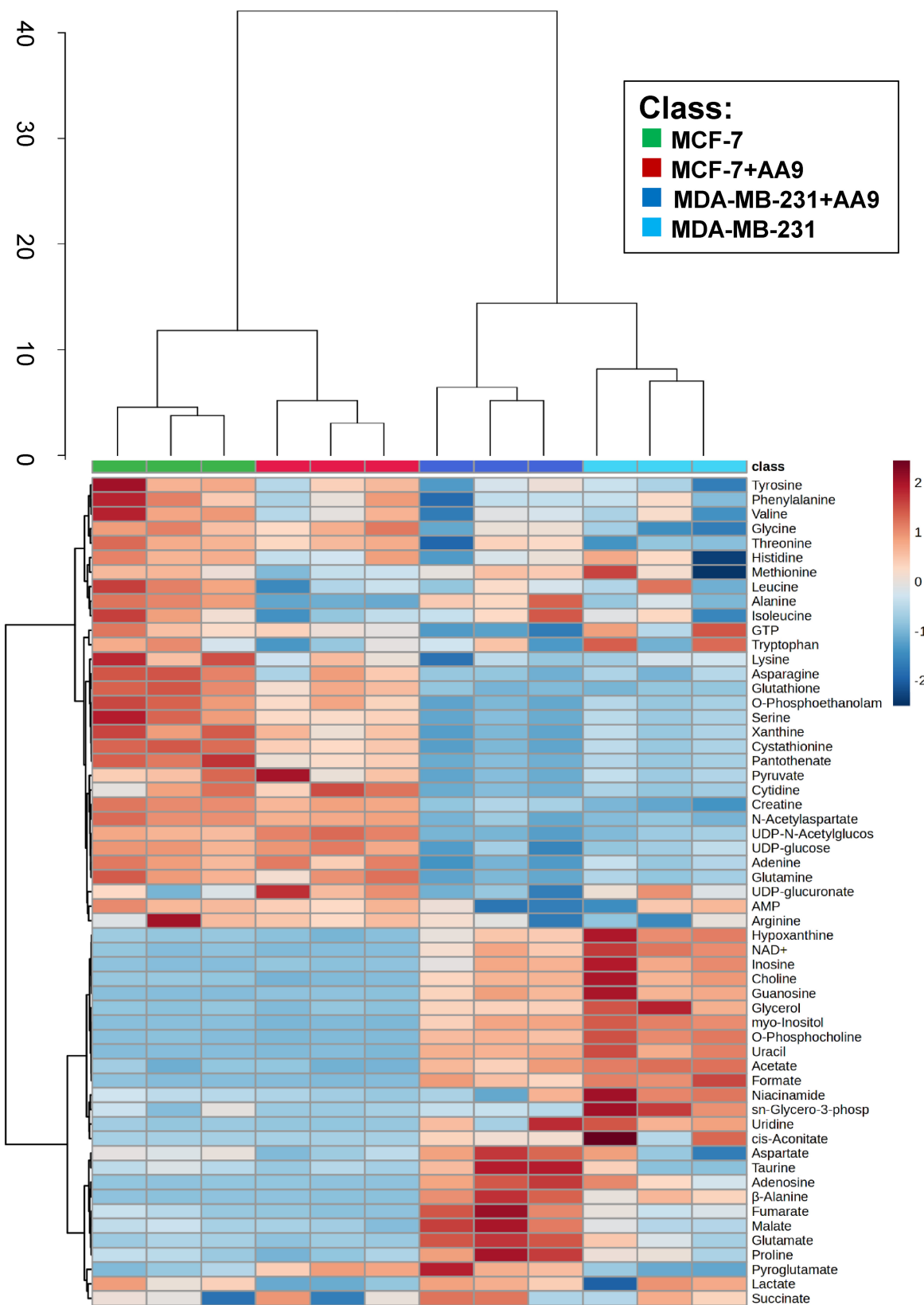
Fig. 4. Hierarchical cluster analysis and heatmap illustrating the metabolite-level datasets. The hierarchical clustering (top) distinguishes four groups of differential metabolic profiles, corresponding to the MD-MB-231 and MCF-7 treated with AA9 or supplemented only with the vehicle and indicated by different colours. In the heatmap (bottom), rows correspond to the identified metabolites, whereas columns correspond to the different triplicate samples derived from independent experiments and characterising each group. On the right, the $\log_2$ scale represents higher (red) and lower (blue) concentrations of metabolites.

the latter reaction can also occur in cell lysate, the interpretation of pyroglutamate concentration is not straightforward as it might represent an artefact not attributable to AA9 action [60]. For this reason, we will not discuss it further.

Metabolic alterations induced by AA9 inhibitor on MDA-MB-231 cells

The pathway topological analysis, shown in Fig. 8A, points to 12 dysregulated pathways ($P < 0.01$ and pathway impacts > 0.1, Fig. 8B). Those with pathway impact > 0.4 are alanine, aspartate, and glutamate metabolism; glutamine and glutamate metabolism; nicotinate and nicotinamide metabolism; taurine and hypotaurine metabolism; and β-alanine metabolism.

Among the numerous metabolites indicated to undergo a remarkable concentration change and reported in Fig. 5D, glutamate is present in 7 out of 12 of the metabolic pathways significantly affected by AA9 in Fig. 8B, namely: glutathione metabolism; arginine and proline metabolism; nicotinate and nicotinamide metabolism; glutamate and glutamine metabolism; alanine, aspartate, and glutamate metabolism; glyoxylate metabolism; and arginine biosynthesis. Aspartate is present in four pathways (together with glutamate in three of them): nicotinate and nicotinamide metabolism; alanine, aspartate, and glutamate metabolism; arginine biosynthesis; and glycine, serine, and threonine metabolism, in which glutamate is not present. All the remaining metabolites, shown in Fig. 5D, can be spotted in one of the significantly altered metabolic pathways reported (Fig. 8B).

Using the same criteria as for the MCF-7 cell line, we generated a volcano plot for MDA-MB-231 cells (Fig. 9A). The box plots, shown in Fig. 9B, highlight the metabolites with significantly altered concentrations: (a) an increase of the amino acids aspartate, proline, and glutamate, together with the amino acid derivatives taurine, β-alanine, and creatine; (b) an increase of fumarate, malate, and adenosine; (c) a decrease in GTP, hypoxanthine, niacinamide, and *sn*-glycero-3-phosphocholine.

Fumarate (alanine, aspartate, and glutamate metabolism) and malate (glyoxylate and dicarboxylate metabolism) are also associated with the pyruvate and

Krebs pathways, which, despite not having a pathway impact > 0.1 in our analysis, still have a significant P-value and a good FDR.

As for choline and *O*-phosphocholine, despite their significant VIP scores (Fig. 5D), 1.37 and 1.25, respectively, they are not among the metabolites that satisfy the selection rules of the volcano plot (Fig. 9).

To summarise, TG2 inhibition primarily impacts amino acid, pyruvate, Krebs cycle, and purine metabolisms.

Comparison of metabolites and pathways affected by AA9 in MCF-7 and MDA-MB-231 cell lines

The volcano plots (Fig. 7 and Fig. 9) show that AA9 exerts a diverse effect on the metabolome of the two cell lines, with a larger number of metabolites with significantly altered concentrations in MDA-MB-231 than in MCF-7 cells.

Interestingly, the VIP scores in Fig. 5C,D, reveal three common metabolites: choline, *O*-phosphocholine, and myo-inositol. Myo-inositol shows a higher score in MCF-7 than in MDA-MB-231 cells (1.33 *vs*. 1.25). The pathway analysis of the two cell lines, Fig. 6 and Fig. 8, shows that the inositol phosphate metabolism is perturbed in both with a pathway impact of 0.13 and a statistical relevance with $-\log(P)$ values of 2.59 and 2.01 for MCF-7 and MDA-MB-231 cells, respectively.

An alteration in purine metabolism, highlighted by the increase in guanosine levels in MCF-7 (Fig. 6), is not evidenced in the pathway analysis of MDA-MB-231 cells (Fig. 8), despite the significant alterations observed for adenosine, hypoxanthine, and GTP (Fig. 9).

The VIP scores of MCF-7 cells do not highlight fumarate or malate. However, the pathway analysis shown in Fig. 6B indicates the pyruvate metabolism (FDR = 0.046, pathway impact 0.30, $-\log(P)$ of 2.01), to which fumarate is linked. Instead, fumarate is identified, with a VIP score of 1.29 (Fig. 5D), only for the MDA-MB-231 cells reflecting alteration of the alanine, aspartate, and glutamate metabolisms (FDR = 0.024, pathway impact 0.24 and $-\log(P)$ of 2.27). Similarly, although malate is not among the 15 metabolites with higher VIP scores for MCF-7, in MDA-MB-231 cells presents a high VIP score of 1.34 belonging to the glyoxylate and dicarboxylate metabolism (Fig. 8).
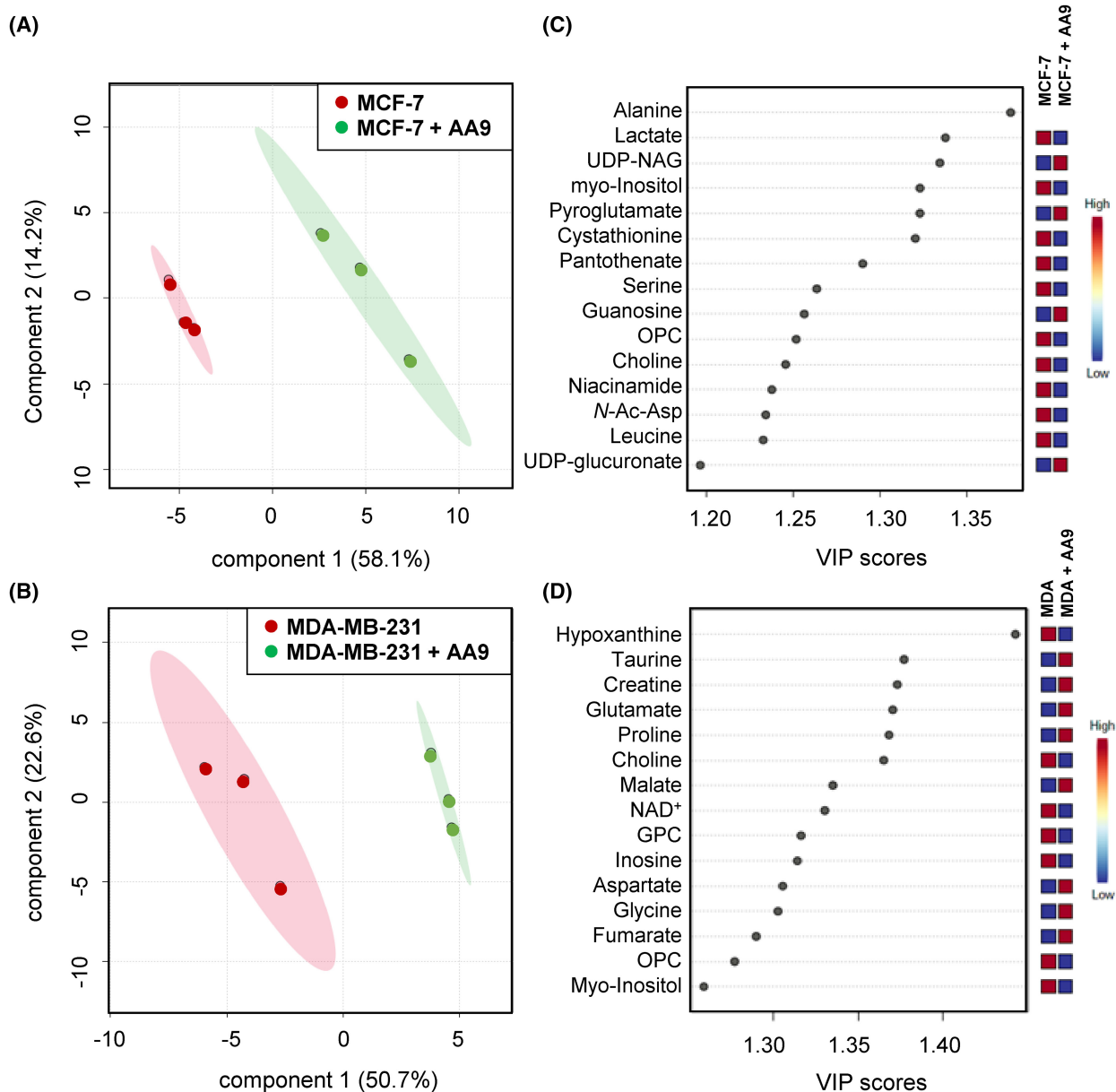
Fig. 5. On the left, PLS-DA plot of the intracellular metabolome of MCF-7 (A) and MDA-MB-231 (B) cell lines with and without the TG2 inhibitor AA9. The plots are the result of three independent replicates. Before analysis, metabolite concentrations were normalised by the median concentration of each sample and auto-scaled (mean-centred and divided by the SD of each variable). On the right are the 15 top metabolites separating by component 1 in the PLS-DA plots for MCF-7 (C) and MDA-MB-231 (D) cells. Higher VIP scores indicate relevant contributions to discriminating between the groups. The coloured boxes (red and blue) on the right side of the VIP score plot denote the relative metabolite abundance in each cluster of the PLS-DA. GPC, *sn*-glycerophosphocholine; N-Ac-Asp, *N*-acetyl-aspartate; OPC, *O*-phosphocholine; UDP-NAG, UDP-*N*-acetylglucosamine.

Discussion

AA9 is a novel inhibitor derived from NC9, which has raised much interest. To investigate the molecular mechanisms that govern its action, we selected MCF-7 and MDA-MB-231 as BrCa reference cell lines.

The ability to enter the cells and persist inside is one of the important features that an anticancer drug must possess. The permeability data indicate that AA9 has good passive permeability and better performance than NC9. In MDA-MB-231 cells, AA9 permeability agrees with its good efficacy for *in situ* inhibition of TG2
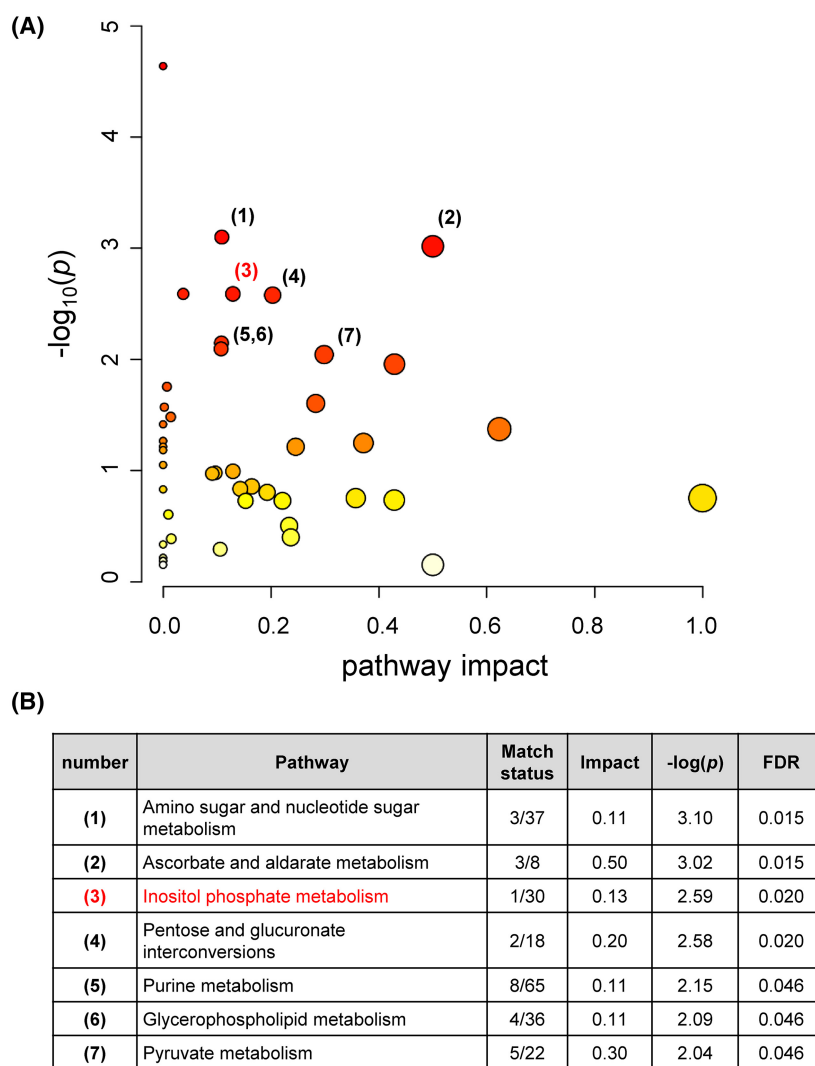
Fig. 6. Pathway analysis of the metabolic changes induced by AA9 in MFC-7 cells. (A) Matched pathways are displayed as circles. The colour of each circle is based on the *P*-value (darker colour indicates more significant changes in metabolites in the corresponding pathway due to AA9 treatment), whereas the size of the circle indicates the pathway impact score. The numbers correspond to the pathways detailed in (B). (B) Summary of the major metabolic pathways altered in MCF-7 cells by AA9 treatment. Metabolic pathways with pathway impact > 0.1 and FDR < 0.05 were considered relevant. In red, is the pathway that MCF-7 cells have in common with MDA-MB-231 cells.

activity, which is higher than that of NC9 used at a concentration close to their K_I. Unfortunately, the assay conditions were unsuitable to detect TG2 activity in MCF-7 cells due, in part, to the low amount of expressed TG2 and the possible internalisation of the BAP substrate. Those adverse effects have been overcome by using more cells and an *in vitro* test of transamidase activity (both on treated cells and on inhibitor-exposed lysates). We can conclude that MCF-7 cells possess transamidase activity that is inhibited by AA9, as inferred by its interference with, albeit low, cell motility. The presence of TG2 [5,61]

and its transamidation activity [62] in MCF-7 cells has already been reported, as well as the alteration of cell motility as a function of TG2 concentration [10].

The great sensitivity of MDA-MB-231 cells to AA9 could also be a consequence of their genetic profile. Based on two sources, the Cancer Cell Line Encyclopaedia (CCLE) (https://sites.broadinstitute.org/ccle/ on February 25, 2022) and the Catalogue of Somatic Mutations in Cancers (COSMIC; https://cancer.sanger.ac.uk/cell_lines on February 25, 2022) and by comparing the mutations to Genome Reference Consortium Human Build 38 (GRCh38/hg38), we found that the
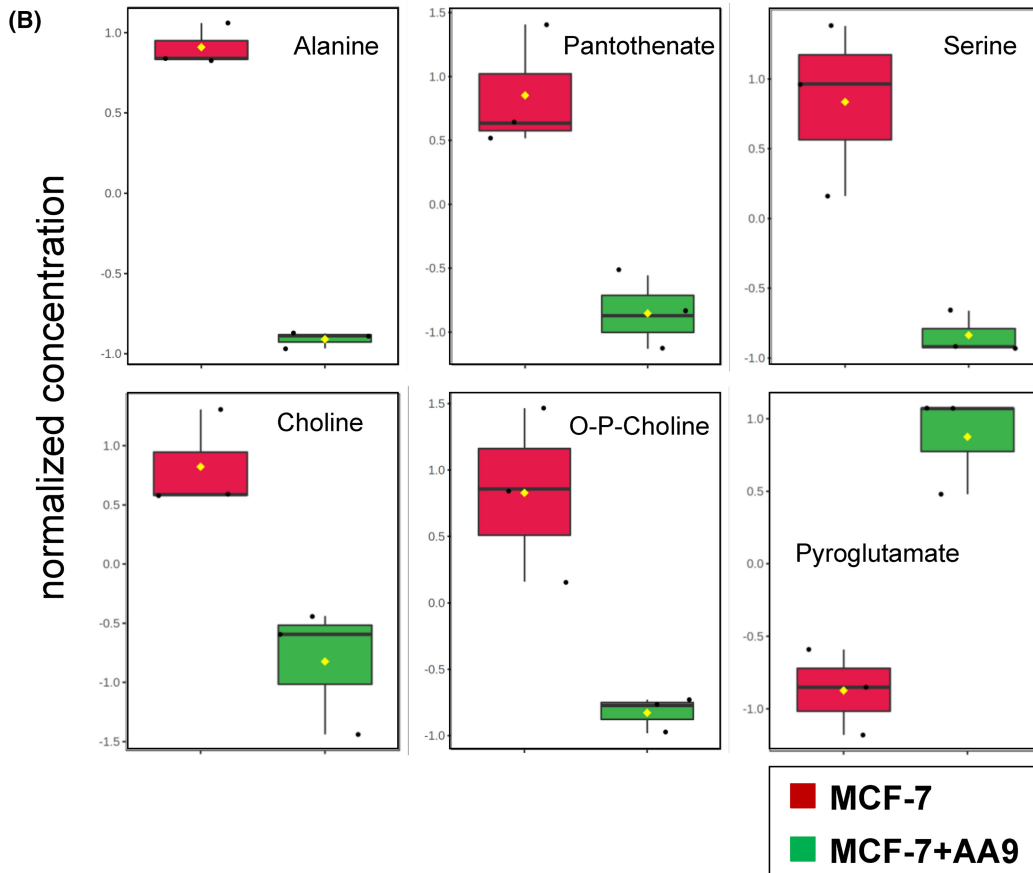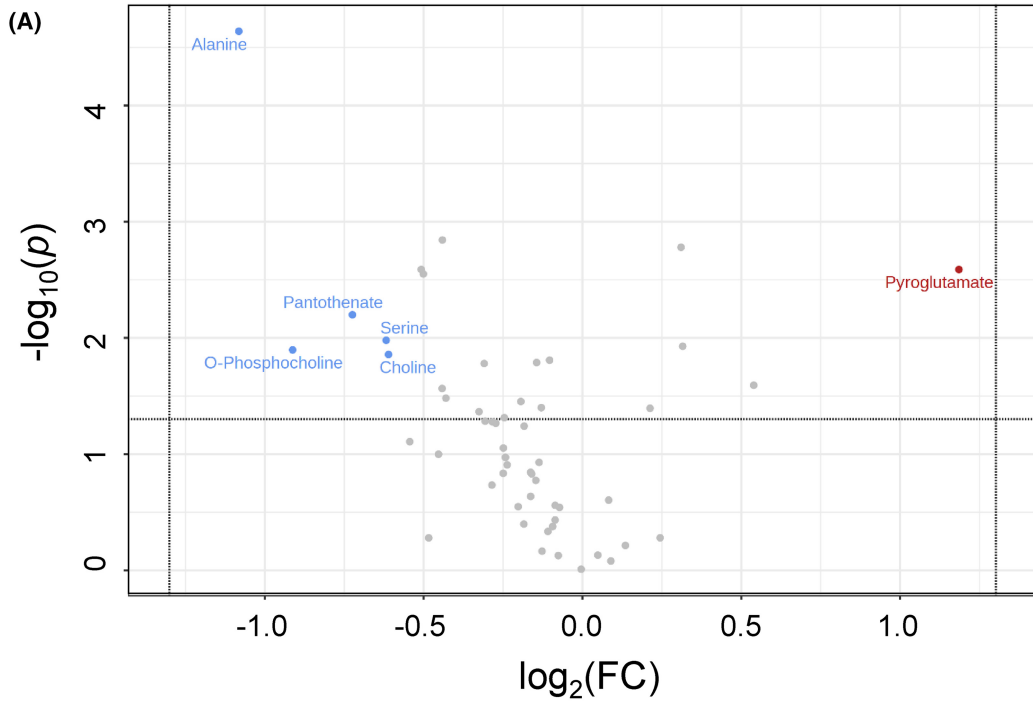
Fig. 7. Univariate analysis of the intracellular metabolome obtained from MCF-7 cells treated with AA9 versus untreated cells. (A) Volcano plot analysis based on fold change |FC| > 1.5 and a *P* value < 0.05, reported as a logarithmic scale. The red, blue, and grey dots represent up-regulated, down-regulated, and insignificantly changed metabolites in AA9 treated versus untreated cells, respectively. (B) Box and whisker plots of the significant metabolites differentially expressed in untreated MCF-7 cells (red) or treated with AA9 (green). The univariate statistical analysis corresponds to three independent experiments. Before analysis, metabolite concentrations were normalised by the median concentration of each sample and auto-scaled (mean-centred and divided by the SD of each variable). O-P-choline, *O*-phosphocholine.

triple-negative MDA-MB-231 cells are mutated in ABC transporter genes (ABCA3 and ABCC1), which contribute to the fluxes of molecules across the plasma membrane [63]. We underline that the efflux ratio of AA9 improved when combined with the Pgp inhibitor Zosuquidar [53], thus supporting our hypothesis and representing a relevant point considering its use in multi-drug therapeutic protocols [10,25–29].

Considering that NC9 can contrast cell migration in both cell lines [10], we tested only AA9. Our findings using the xCELLigence RTCA system demonstrated the good potential of this compound to limit migration within 24 h, with a more significant effect in MDA-MB-231 cells. Moreover, AA9 reduces the invasiveness of MDA-MB-231. This latter aspect was not evaluated in MCF-7 cells because they are not endowed with a marked invasive ability [10].
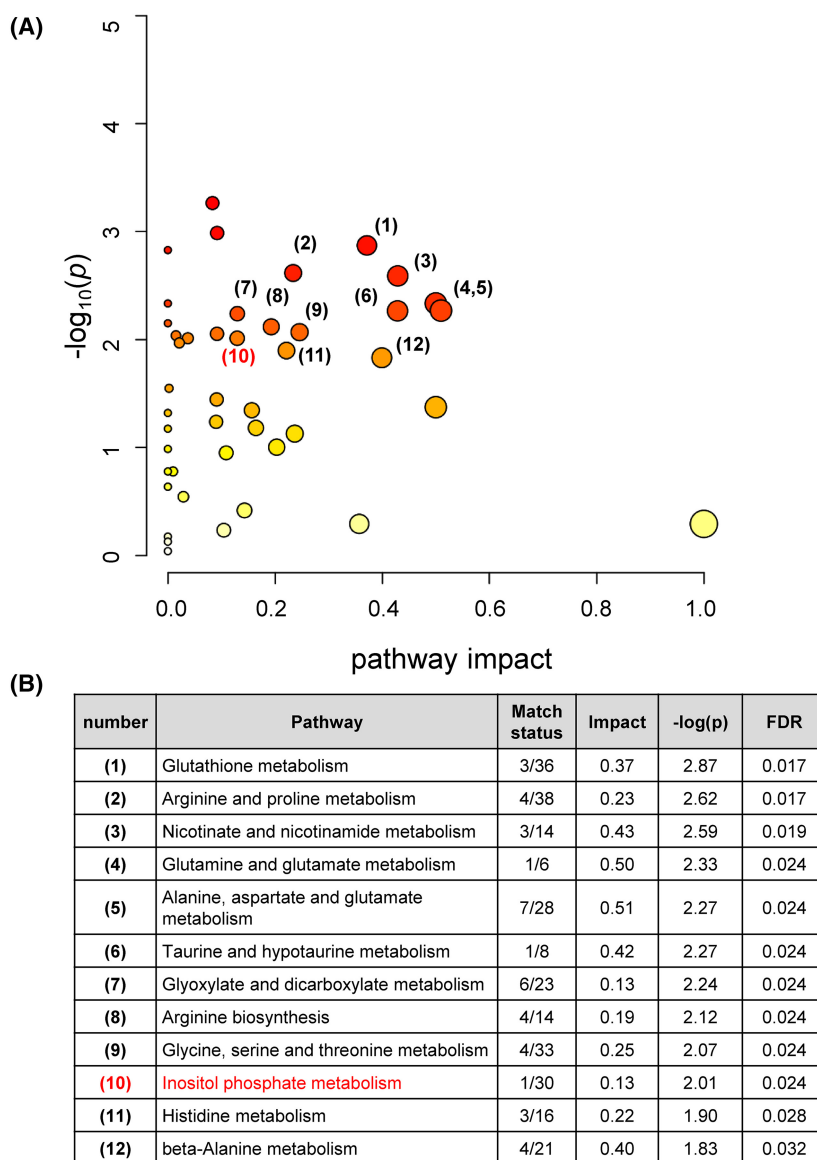
Prevention of cancer cell movement does not only stop the tumour from spreading but also helps to sensitise them to an anticancer effect. Accordingly, we tested NC9 and AA9 inhibitors for apoptosis induction in both cell lines. Despite the presence of an acrylamide group that may allow for off-target reactivity, this event does not necessarily occur if the design of the compound accurately guides the inhibitor to its target [30]. We found that, after a treatment of 48 h at the lowest tested concentration (25 μM), AA9 produced the highest apoptosis percentage in MDA-MB-231 cells. While both NC9 and AA9 induced dose-dependent apoptotic effects in MCF-7 cells, the lack of a comparable dose-dependent increase in MDA-MB-231 cells could be attributed to the inhibitors' moderate permeability, high efflux ratio, or biotransformation. These pharmacokinetic properties are the focus of ongoing research aimed at developing these inhibitors into more effective drugs [64]. Even if the pro-apoptotic effect is moderate, the interest in TG2 inhibitors is mainly due to their potential use in combination with other chemotherapeutic agents [23,26].

Several recent metabolomics studies have been performed on MDA-MB-231 and MCF-7 cell lines to test the effects of different anticancer treatments [42,43,46,47,49,65].

The characterisation of the metabolic impact due to AA9 inhibition of TG2 highlighted a significant number of metabolites, supporting the concept that AA9 drives metabolic modifications in a cell line-specific manner.

AA9 treatment of MCF-7 cells significantly decreases alanine, serine, choline, *O*-phosphocholine, and pantothenate. The decrease in serine concentration is expected to limit the proliferation rate because serine biosynthesis supports BrCa cell growth [66]. A decrease in serine should affect the metabolism of folic acids and serine palmitoyltransferase activity, which, by catalysing the biosynthesis of sphingosine (a precursor of sphingolipids and non-canonical 1-deoxysphingolipids) [67], may alter the membrane composition, thus limiting tumour growth and progression. Phospholipid metabolism is strongly associated with oncogenesis, and interference with the levels of choline and *O*-phosphocholine is expected to impact membrane turnover [58,68]. This finding is consistent with the observation that *O*-phosphocholine and choline levels decrease after AA9 treatment in both cell lines, even though significant changes in the glycerophospholipid metabolism occur only in MCF-7 cells. Indeed, gene mutations affect glycerophospholipid metabolism and choline uptake in BrCa [67]. Interestingly, phosphocholine and choline content are the results of two pathways: phosphocholine synthesis, due to choline kinase upregulation in the Kennedy biosynthetic pathway, and phosphatidylcholine degradation, mediated by phospholipase C [68]. The latter is notoriously regulated by TG2 through its G-protein function [21,56,68,69] and may be altered by AA9 [32]. This function has been associated with metastatic progression in triple-negative BrCa [70].

We underline that MDA-MB-231 cells are more sensitive to the action of AA9, as shown by the volcano plot, displaying a wider range of altered metabolites. Amino acid levels are significantly modified, with notable increases in glutamate and aspartate, along with β-alanine. Cancer cellular metabolic reprogramming responds to an increased demand for amino acids to produce energy and re-synthesise proteins,

(A)

(B)

number	Pathway	Match status	Impact	-log(p)	FDR
(1)	Glutathione metabolism	3/36	0.37	2.87	0.017
(2)	Arginine and proline metabolism	4/38	0.23	2.62	0.017
(3)	Nicotinate and nicotinamide metabolism	3/14	0.43	2.59	0.019
(4)	Glutamine and glutamate metabolism	1/6	0.50	2.33	0.024
(5)	Alanine, aspartate and glutamate metabolism	7/28	0.51	2.27	0.024
(6)	Taurine and hypotaurine metabolism	1/8	0.42	2.27	0.024
(7)	Glyoxylate and dicarboxylate metabolism	6/23	0.13	2.24	0.024
(8)	Arginine biosynthesis	4/14	0.19	2.12	0.024
(9)	Glycine, serine and threonine metabolism	4/33	0.25	2.07	0.024
(10)	Inositol phosphate metabolism	1/30	0.13	2.01	0.024
(11)	Histidine metabolism	3/16	0.22	1.90	0.028
(12)	beta-Alanine metabolism	4/21	0.40	1.83	0.032

Fig. 8. Pathway analysis of the metabolic changes induced by AA9 in MDA-MB-231 cells. (A) The numbers correspond to the pathways detailed in (B). (B) Summary of the major metabolic pathways altered in MDA-MB-231 cells by AA9 treatment. Metabolic pathways with pathway impact > 0.1 and FDR < 0.05 were considered relevant. Inositol phosphate metabolism (in red) is significantly affected by AA9 both in MDA-MB-231 and MCF-7 cells.

Fig. 9. Univariate analysis of the intracellular metabolome obtained from MDA-MB-231 cells treated with AA9 versus untreated cells. (A) Volcano plot analysis based on fold change |FC| > 1.5 and a *P* value < 0.05, reported as a logarithmic scale. The red, blue, and grey dots represent up-regulated, down-regulated, and insignificantly changed metabolites in AA9- versus control cells, respectively. (B) Box and whisker plots of the significant metabolites differentially expressed in untreated MDA-MB-231 cells (red) or treated with AA9 (green). The univariate statistical analysis corresponds to three independent experiments. Before analysis, metabolite concentrations were normalised by the median concentration of each sample and auto-scaled (mean-centred and divided by the SD of each variable). *sn*-GPC, *sn*-glycerophosphocholine.

(A)

(B)
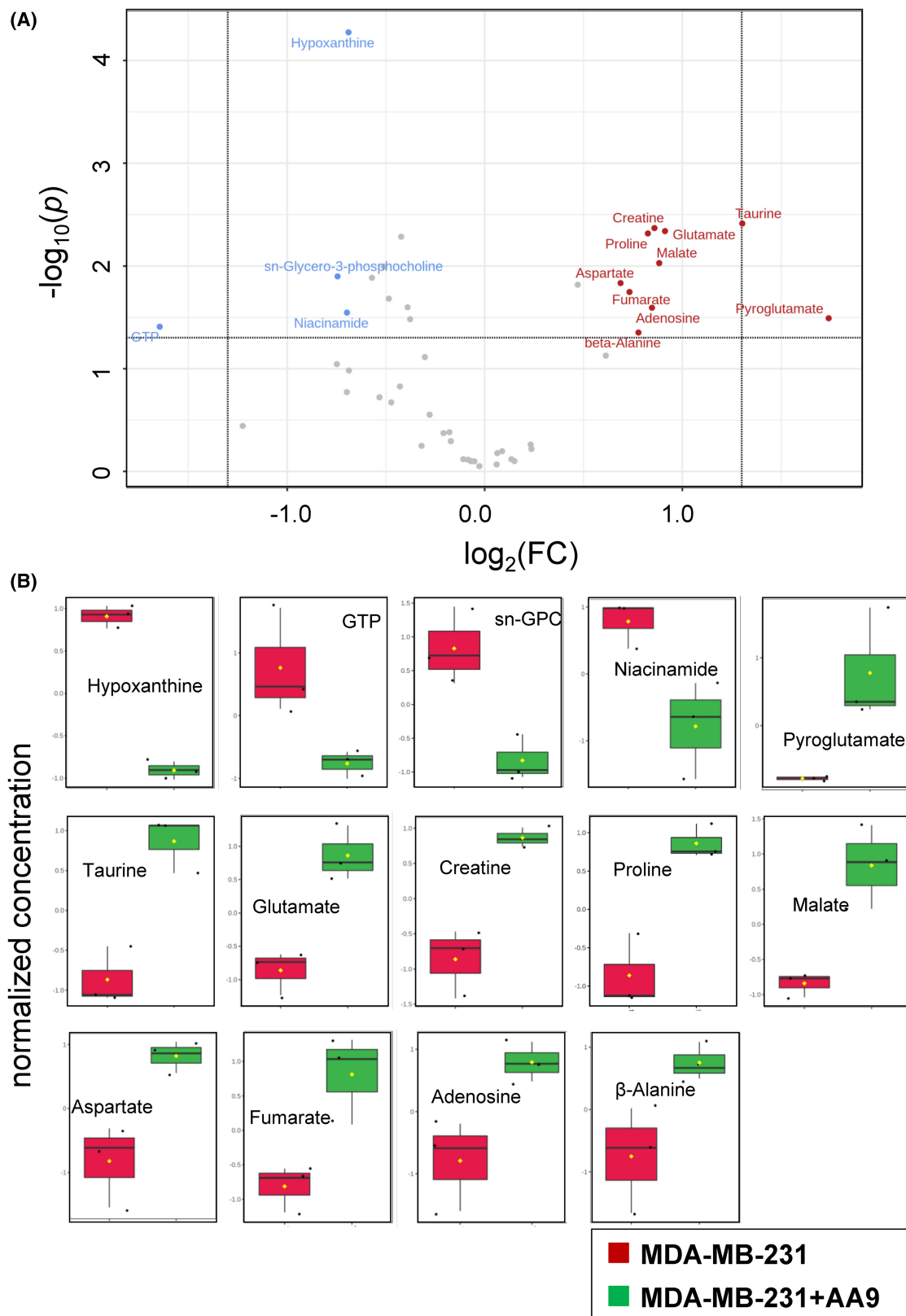
maximising amino acid uptake from the extracellular environment. This request is associated with modifications that affect the metabolism of pyruvate and the Krebs cycle, which, especially in MDA-MB-231 cells [16], might involve modifications of specific enzymes that have been reported to be substrates of TG2, such as glyceraldehyde-3-phosphate dehydrogenase, α-ketoglutarate dehydrogenase [17,18], and aldolase and cytochrome c [18]. This finding might reflect alterations of mitochondrial functions relevant to apoptosis [71], as also proved by the adenylate translocator, a substrate of TG2 [72].

To summarise, our data display preferential alteration of membrane turnover in MCF-7 in contrast to amino acid metabolism in MDA-MB-231 cells. AA9 limits energy consumption and nucleotide metabolism, selectively impacting the concentration of specific metabolites. In MCF-7 cells, purine metabolism is included among the significantly dysregulated pathways, while volcano plot analysis of MDA-MB-231 cells showed decreasing GTP and hypoxanthine, which belong to the purine metabolism pathways. With predictive significance, the concentration of hypoxanthine is of fundamental importance [73].

Since these cell lines have different mutations, the observed metabolic changes might be conditioned by their specific genomic framework [51]. MDA-MB-231 cells have a missense mutation for ACO1 (the aconitase 1 gene), which may exacerbate the imbalance induced by AA9 in Krebs intermediates. The mutation in MDA-MB-231 cells of the SLC27A1 (Solute carrier family 27 member 1) gene, coding a transporter of long-chain fatty acids involved in glycerophospholipid biosynthesis, could affect *sn*-glycero-3-phosphocholine levels in these cells. On the other hand, SLC5A7 (solute carrier family 5 member 7), which mediates choline uptake, is mutated in MCF-7 cells. Another player in the glycerophospholipid balance could be PLA2R1 (phospholipase A2 receptor 1), which negatively regulates the secretion of PLA2 and is responsible for the cleavage of glycerophospholipids. Since TG2 acts as an activator of PLA2 [19,20], AA9 could influence this pathway. Concerning the MCF-7 cell genome, the mutations interfering with the phosphatidylinositol signalling system and affecting PIK3AP1 (phosphoinositide-3-kinase adaptor protein 1) and PIK3CA (phosphatidylinositol-4,5-bisphosphate 3-kinase catalytic subunit alpha) might modify the myo-inositol concentration and the glycerophospholipid metabolism. These mutations could emphasise the effects of AA9 on the two cell lines, impacting the Krebs cycle and glycerophospholipid metabolism in MDA-MB-231 and phosphatidylinositol signalling in MCF-7 cells.

Despite their different genomic features, we have identified a common, significantly deregulated pathway, the inositol phosphate metabolism. AA9 treatment causes an increase in myo-inositol concentration in MDA-MB-231 cells containing higher levels of TG2. Currently, myo-inositol is suggested as an adjuvant in treating several diseases [74]. Myo-inositol perturbation has been associated with the antineoplastic effects of chemotherapeutic drugs, such as cisplatin [75]. The relevance of myo-inositol in BrCa therapy is demonstrated by the improvement of quality of life, ameliorating the symptoms of patients when co-administered with chemotherapy [76].

We emphasise the importance of supplementing traditional therapies with new molecules that could reduce the dosage and toxicity of anticancer drugs while limiting the invasiveness and infiltration features that make BrCa treatment a challenge [40]. In this regard, AA9 may be a promising candidate whose potential should be further investigated. Clearly, in our experimental conditions, as with all assays involving the administration of drugs, off-target effects cannot be ruled out. Further investigations to identify proteins non-specifically interacting with AA9 are required to better understand the *in vivo* mode of action of this TG2 inhibitor.

The metabolomic approach, which focuses on a qualitative and quantitative analysis of the intracellular metabolites, is particularly powerful. The observed metabolic effects following the TG2 inhibitor administration might be due to both transglutaminase and signal cascade interference. We envisage expanding our investigation to elucidate the partners and pathways influenced by TG2 inhibitors, as well as the involvement of this enzyme in the pathogenesis of BrCa.

Conclusions

Perturbations of the metabolomes of BrCa hormone-sensitive MCF-7 and triple-negative MDA-MB-231 cells caused by the novel TG2 inhibitor AA9 have been investigated using ^{1}H-NMR. Because of the multifunctional roles of TG2, AA9 alters the concentration of several metabolites in both BrCa cell lines, impacting specific cellular pathways. AA9 appears more effective on MDA-MB-231 cells, as evaluated by metabolomic perturbations and migration inhibition. We believe this differential effect is due to: (a) the genomic assets of the two cell lines; (b) the higher level of TG2 expression in MDA-MB-231 compared to MCF-7 cells; and (c) the inhibitor membrane permeability, efflux ratio, or time-dependent biotransformation within the cells.

In the context of the large diversity that characterises these two cell lines, the effects on inositol phosphate metabolism might be a valuable key to unveiling the molecular mechanisms that underlie AA9 activity.

Materials and methods

Transglutaminase 2 inhibitors

The two inhibitors, AA9 and NC9, were synthesised as described previously [17]. Their chemical names are (*S*)-benzyl (1-(4-(1-naphthoyl)piperazin-1-yl)-6-acrylamido-1-oxohexan-2-yl)carbamate and *N*-α-carbobenzyloxy-*N*-ε-acryloyl-L-lysine (2-(2-dansylaminoethoxy)-ethoxy)ethanamide, respectively. Stock solutions were stored at $-20\ °C$, at 300 mM concentration in DMSO 10% and diluted immediately before use. These compounds are also commercially available from ZEDIRA GmbH (Darmstadt, Germany).

Permeability assays

The in vitro pharmacokinetic properties of AA9 and NC9 were evaluated by Pharmaron, Inc. (Louisville, KY, USA). Passive diffusion across a lipid membrane was measured in a PAMPA using 1.8% lecithin in dodecane as the artificial membrane and measuring diffusion after 16 h of incubation at 25 °C. To measure diffusion through a cell layer, Madin-Darby canine kidney cells transfected to express Pgp were grown to confluence on transwell membranes, and the integrity of the cell layer was verified by transepithelial electrical resistance. The assays were carried out by adding the molecules to either the apical or basolateral compartments, and the assembled transwell plates were incubated for 2 h at 37 °C. At the end of the transport period, the concentrations of inhibitors in the upper and lower chambers were determined by liquid chromatography-mass spectrometry.

Cell culture conditions and treatments

In this perspective, MCF-7 cells are oestrogen and progesterone receptor-positive and human epidermal growth factor receptor 2 (HER2)-negative, belong to the luminal A subtype. They have an irregular cuboid shape, as well as a low tendency to metastasize, often used to check the development of drug resistance [10,77]. While the triple-negative MDA-MB-231 cells, despite showing an epithelial origin, display a mesenchymal-like phenotype with a spindle shape and manifest a high propensity to invasion and metastasization [78].

The BrCa-derived MCF-7 (RRID: CVCL_0031) and MDA-MB-231 (RRID: CVCL_0062) cells were purchased from the American Type Culture Collection (Rockville, MD, USA). Both cultures were tested monthly for contamination by mycoplasma and other microorganisms and subjected to cell identification by single-nucleotide polymorphism quarterly. In addition, we analysed the gene expression of the two cell lines by RNA sequencing, and the results were compared with data obtained from the GEO NCBI database (https://www.ncbi.nlm.nih.gov/geo/, GSE154809 for MDA-MB-231, and GSE111151 for MCF-7). The top 5 genes (*LRR1*, *SNAPC5*, *PELO*, *PGK1*, *SEC61A1* for MDA-MB-231 and *KRT8*, *SDHD*, *TBCA*, *PGD*, and *CCND1* for MCF-7 cells), indicating the highest model-specific effect-size expression and associated with loss of fitness, demonstrated comparable scores. These genes, calculated as indicated by Project Score (Wellcome Sanger Institute database, https://www.sanger.ac.uk/tool/project-score-database/), represent those that more characterise the biological activity and the phenotype of each cell line.

MCF-7 cells were cultured at 37 °C in a 5% CO_2 humidified atmosphere in Dulbecco's Modified Eagle Medium (DMEM, GE-Healthcare, Milano, Italy), supplemented with 10% foetal bovine serum (Gibco Laboratories, New York, NY, USA), 2 mM L-glutamine (Merck Life Science, Milan, Italy), 50 $U\cdot mL^{-1}$ penicillin, and 50 $\mu g\cdot mL^{-1}$ streptomycin (Merck Life Science). MDA-MB-231 cell cultures were grown in similar conditions but using DMEM High Glucose w/stable L-glutamine (EuroClone, Pero, Italy) with the addition of the same antibiotics. Cells were grown in triplicate for all tested conditions using T75 flasks (Euro-Clone), reaching around 70% confluence before any treatment. At this stage, the culture medium was removed and replaced by a fresh medium; after 8 h of adaptation to culture conditions, cells were exposed to a specific TG2 inhibitor for 16 h according to the experimental procedure previously developed for these cell lines [10]. Cell cultures were treated using either 9 μM AA9 or 30 μM NC9 in 0.1% DMSO, corresponding to their K_I values. As a reference, cell cultures were grown in a medium supplemented with 0.1% DMSO.

Gene expression quantification by RT-qPCR

We used TRI Reagent® to extract total RNA from 3×10^6 cells, as reported in the manufacturer's protocol (Merck Life Science). One microgram of total RNA was reverse transcribed using the TaqMan® Reverse Transcription Reagents Kit (Thermo Fisher Scientific, Monza, Italy) and quantitative polymerase chain reactions (qPCRs) were carried out as reported by Franzese *et al.* [79]. Fold change was calculated applying the formula $2^{\Delta CT}$, where ΔCT value was the difference between the CT mean and the CT of the specific sample, then normalised using the geometric mean of two references, β-actin (forward primer 5′-CATTGCCGACAGGATGCA-3′, reverse primer 5′-GCTGATCCACATCTGCTGGA-3′) and GAPDH (forward

primer 5′-CTATAAATTGAGCCCGCAGCC-3′, reverse primer 5′-CCCAATACGACCAAATCCGT-3′).

In situ TG2 activity analysed in MDA-MB-231 cells

To assay the block of catalytic activity of TG2 in the BrCa cells, we modified and adjusted the protocol described by Verhaar *et al.* [54]. We seeded the cells in T25 flasks. At about 80% confluence, the supernatant from each sample was gently removed without detaching the cells and discarded. We then washed the cells with 5 mL of culture medium (without FBS and antibiotics), adding it drop by drop and taking care not to detach the cells. To each flask or sample, we added 1.5 mL of culture medium, containing 1 mM *N*-(5-aminopentyl)biotinamide trifluoroacetate salt (BAP, 10 mM concentrated stock solution, Merck Life Science S.r.l., Milano Italy). After an incubation of 4 h, we treated with TG2 inhibitors, while the control was represented by the treatment with 0.1% DMSO (the solvent in which the inhibitors were resuspended) for 1 h, followed by the addition of 10 μM A23187 (Merck Life Science S.r.l.) as the final concentration for 90 min. Also, we detached the cells using a scraper, transferred them to a 1.5 mL Eppendorf tube, and collected each sample by centrifugation at 300 g for 5 min. We washed twice with 1.5 mL of cold PBS and transferred the pellet into a 0.5-mL Eppendorf tube, and finally resuspended it in 200 μL of cold homogenising buffer (TRIS 50 mM, NaCl 150 mM, EDTA 1 mM; protease inhibitors (Halt™ Protease Inhibitor Cocktail Thermo Fisher Scientific) 1 μg·mL⁻¹ pH = 7.4, and phenylmethylsulfonyl fluoride (0.1 mM added at time of use). The lysates could be stored at −80 °C, sonicate (in immersion 5 s pulse + 5 s pause for 5 times). Cellular extracts have been quantified by the Bradford Protein Assay.

Ten micrograms of homogenate were diluted to 50 μL with coating buffer (50 mM Tris-HCl, pH 7.4, 150 mM NaCl, 5 mM EGTA, 5 mM EDTA), dispensed into wells of a 96-well microtiter plate for ELISA (Maxisorp Nunc ImmunoPlate, Thermo Fisher Scientific) and incubated overnight at 4 °C. After three washing steps with 300 μL per well of washing buffer (0.1 M Tris-HCl, pH 8.5), the non-specific sites were saturated with 300 μL per well of 5% BSA prepared in 150 mM NaCl, 10 mM NaH₂PO₄, pH 7.2, 0.05%v/v Tween-20 (blocking diluent) for 1 h at room temperature, applying gentle agitation. After three washing steps with 300 μL per well of the same buffer, 100 μL of HRP-conjugated streptavidin (1 : 2000 diluted in blocking diluent) was added to each well, and the plate was incubated for 20 min at room temperature by gentle shaking. Finally, after five washes with 300 μL per well, 100 μL per well of substrate mix was added (0.42 mM 3,3′,5,5′-tetramethylbenzidine, 1.95 mM hydrogen peroxide, dissolved in 20 mM sodium citrate, pH = 5), and the incubation was performed at room temperature for 10–20 min in the dark with gentle shaking. The reaction was stopped by adding 100 μL of 2 M H₂SO₄, and the wells were read in a microplate reader (Tecan Infinite M200, Tecan, Hombrechtikon, Switzerland) at 450 nm with a reference set at 540 nm. All measurements were done in triplicate and repeated at least three times.

The amounts of BAP-associated proteins were calculated as percentage with respect to the control treated with 0.1% DMSO.

In vitro transamidation activity analysed in MCF-7 cells

To investigate the effects of TG2 inhibitors in MCF-7 cells, they were grown in t75 flasks using the above-reported culture conditions. In one set of experiments, we treated MCF-7 cells with the compounds for 1 h. Next, cell pellets were collected, washed with PBS 1×, and centrifuged at 1200 r.p.m. for 5 min, then resuspended in 200 μL of cold homogenising buffer, sonicated, and quantified. Also, a major amount (25 μg) of total lysate has been analysed for transamidase activity. In the second set of experiments, we harvested the cells and produced the homogenates, but in this case, we directly exposed 25 μg of lysate to the action of a 10 μM AA9 inhibitor while performing a control test without the inhibitor. Finally, the transamidation assay was carried out as follows. The homogenates were incubated in assay buffer containing 10 mM DTT, 10 mM CaCl₂, and 0.1 M Tris-HCl pH 8.1 at 37 °C, and BAP was added at the final concentration of 2 mM and incubated for 1 h at 37 °C. The reaction was stopped by adding 10 mM EDTA. An ELISA plate was loaded with the extracts, and the colorimetric HRP-conjugated streptavidin reactions were carried out as above described.

Cell migration and invasion assays

Migration and invasion properties of collected cells were analysed by the xCELLigence RTCA system (Real-Time Cell Analyser System, Acea Biosciences Inc., San Diego, CA, USA) [10]. About 4×10^5 cells per well were deposited onto the top chamber of CIM-16 plates. The assay of invasiveness was carried out using diluted Matrigel (1 : 20 in serum-free medium, BD Biosciences, Milan, Italy) layered in the upper chamber, while medium containing 10% FBS was used as a chemoattractant in the bottom chamber in the invasiveness assay or at 5% FBS in the migration assay. Each measurement was performed in quadruplicate, detecting the signal every 15 min for 24 h. Impedance values were indicated as a dimensionless parameter (Cell Index, CI), and values greater than 0.1 were considered positive. Finally, the rate of cell movement was quantified by calculating the slope, indicating the steepness, inclination, gradient, and changing rate of the CI curves over time.

Apoptosis assay

Cells were seeded in 2-mL wells, exposed for 48 h to TG2 inhibitors, trypsinised, and resuspended in PBS solution with 10% FBS. The apoptotic effects were evaluated in samples of 1×10^5 cells using the Muse® Annexin V and Dead Cell Kit (Luminex, Prodotti Gianni, Milan, Italy) as described by Aguiari *et al.* [26].

Cell harvesting and lysis for intracellular metabolite collection

Upon treatment for 16 h, the cell supernatant of each flask was recovered and saved; the treated cells were washed twice with phosphate buffered saline pH = 7.4 (PBS, Thermo Fisher Scientific) and detached by adding 4 mL trypsin-EDTA 0.25% (Thermo Fisher Scientific) and incubated for 5 min at 37 °C. Once cells were detached, confirmed by microscope inspection, and trypsin was inactivated by the addition of the previous supernatant, the cells were resuspended by thoroughly pipetting, collected by centrifugation at 300 *g* for 7 min (4 °C), washed 3 times with 10 mL PBS, resuspended in 10 mL PBS, and analysed by using the cell viability kit and MUSE cell analyser (Prodotti Gianni, Milan, Italy). Reported statistics include % viability and protein content. Finally, cells were pelleted by centrifugation and stored at −80 °C until cell lysis.

Triplicate cell pellets were thawed and suspended in 4 mL of deionised water (4 °C) by vortexing. Cell lysis was affected by sonication, applying two short bursts (30 s) of ultrasound treatment to the cell suspension immersed in an ice bath. To prevent excessive heating, sample tubes were allowed to cool down between the two sonication steps. The absence of intact cells was verified by microscopy inspection.

Fifty microlitres of each lysate were collected for protein quantification (Bradford assay, Sigma-Aldrich, Merck KGaA, St. Louis, MI, USA). The remaining volume of lysate was ultra-filtered using Amicon Ultra-4 Centrifugal filters (10000 MWCO, Merck Millipore, Milan, Italy) at 4000 *g* and 5 °C to deplete the metabolite solution of proteins and cell debris.

The average number (±SD) of cells that have undergone treatment is reported in Table 2, along with the percentage of their viability and the total protein content measured in each lysate before the ultrafiltration step.

Sample preparation and ^{1}H-NMR spectra collection

For NMR sample preparation, each filtered metabolite solution was lyophilised and dissolved in 600 μL of 50 mM phosphate buffer (pH = 7.4), containing 1.45 mM 3-trimethylsilyl propionic acid as a chemical shift reference (0.00 ppm) and quantitative internal standard, and 2.5% D_2O for the signal lock. One-dimensional ^{1}H-NMR spectra were acquired at 25 °C with a JEOL 600 MHz ECZ600R spectrometer (JEOL Inc., Tokyo, Japan) according to the method of Gallo *et al.* [80]. The spectra were processed and analysed with the CHENOMX NMR SUITE 9.0 software (Chenomx Inc., Edmonton, AB, Canada), zero-filling to 256 K points, and processed using a line broadening of 0.5 Hz.

Statistical analyses

NMR metabolite concentrations were normalised by the protein content of each sample. Multivariate statistical analysis was carried out on target metabolites using METABOANALYST 5.0 (https://www.metaboanalyst.ca) [81]. Metabolite concentrations were further normalised by the median and auto-scaled (mean-centred and divided by the standard deviation of each variable) before analysis. PLS-DA was used to compare the metabolite profiles of the two BrCa cells [82]. The hierarchical clustering dendrogram of all 15 samples was performed using the Euclidean distance measure and the Ward algorithm, while the heatmap used the Pearson distance measure and the Ward clustering method. For two-group data analysis, volcano plots were employed, considering 1.5 and 0.05 as FC and raw *P*-value thresholds, respectively.

For pathway analysis, performed with the METABOANALYST 5.0 platform and based on the KEGG pathway database, we used the normalised metabolite concentrations measured in three independent experiments using MCF-7 and MDA-MB-231 cells treated with AA9 or DMSO. The *x*-axis of the pathway analysis plotted in the figures corresponds to the pathway impact value computed by pathway topological analysis, and the *y*-axis is the −log of the *P*-value (−log(*P*)) from pathway enrichment analysis. The most significantly impacted pathways appear in the plot's top-right region.

Acknowledgements

Table 2. Cell treatments and quantitative data of the crude cell lysates. Cell viability and protein quantification are indicated as average values ± SD of three replicate experiments. ªCrude cell lysate

Cell line	Treatment	Cell viability [%]	Protein content[a] [mg_tot]
MCF-7	DMSO	74.1 ± 9.8	40.6 ± 0.4
	AA9	82.7 ± 6.8	43.2 ± 7.0
MDA-MB-231	DMSO	92.1 ± 1.4	10.9 ± 0.7
	AA9	92.4 ± 3.4	8.6 ± 2.7

Conflict of interest

The authors declare no conflict of interest.

Author contributions

NB and TAP were involved in conceptualisation; FB; EF, CT, CMB, NB and TAP were involved in data curation; TAP was involved in formal analysis; SV and NB were involved in funding acquisition; MG, EF, ATe, GA, JWK and NB were involved in investigation; FB, MG, EF, ATe and ATr were involved in methodology; FB, SV and TAP were involved in resources; MG and CT were involved in software; AS, CMB, NB and TAP were involved in supervision; MG was involved in validation; AS, JWK, CMB, NB and TAP were involved in writing—original draft.

Peer review

The peer review history for this article is available at https://www.webofscience.com/api/gateway/wos/peer-review/10.1111/febs.16931.

Data availability statement

All data used to support the conclusions are present in the manuscript.

References

1 Eckert RL, Fisher ML, Grun D, Adhikary G, Xu W & Kerr C (2015) Transglutaminase is a tumor cell and cancer stem cell survival factor. *Mol Carcinog* **54**, 947–958.

2 Kim DS, Park SS, Nam BH, Kim IH & Kim SY (2006) Reversal of drug resistance in breast cancer cells by transglutaminase 2 inhibition and nuclear factor-kappaB inactivation. *Cancer Res* **66**, 10936–109343.

3 Brown KD (2013) Transglutaminase 2 and NF-κB: an odd couple that shapes breast cancer phenotype. *Breast Cancer Res Treat* **137**, 329–336.

4 Agnihotri N, Kumar S & Mehta K (2013) Tissue transglutaminase as a central mediator in inflammation-induced progression of breast cancer. *Breast Cancer Res* **15**, 202–211.

5 Herman JF, Mangala LS & Mehta K (2006) Implications of increased tissue transglutaminase (TG2) expression in drug-resistant breast cancer (MCF-7) cells. *Oncogene* **25**, 3049–3058.

6 Cao J & Huang W (2016) Compensatory increase of transglutaminase 2 is responsible for resistance to mTOR inhibitor treatment. *PLoS ONE* **11**, e0149388.

7 Shinde A, Kulkoyluoglu Cotul E, Chen H, Smit A, Libring S, Solorio L & Wendt MK (2022) Transglutaminase-2 mediates acquisition of neratinib resistance in metastatic breast cancer. *Mol Biomed* **3**, 19–30.

8 Mehta K, Fok J, Miller FR, Koul D & Sahin AA (2004) Prognostic significance of tissue transglutaminase in drug resistant and metastatic breast cancer. *Clin Cancer Res* **10**, 8068–8076.

9 Karicheva O, Rodriguez-Vargas JM, Wadier N, Martin-Hernandez K, Vauchelles R, Magroun N, Tissier A, Schreiber V & Dantzer F (2016) PARP3 controls TGFβ and ROS driven epithelial-to-mesenchymal transition and stemness by stimulating a TG2-snail-E-cadherin axis. *Oncotarget* **7**, 64109–64123.

10 Bianchi N, Brugnoli F, Grassilli S, Bourgeois K, Keillor JW, Bergamini CM, Aguiari G, Volinia S & Bertagnolo V (2021) The motility and mesenchymal features of breast cancer cells correlate with the levels and intracellular localization of transglutaminase type 2. *Cell* **10**, 3059–3078.

11 Beninati S, Piacentini M & Bergamini CM (2017) Transglutaminase 2, a double face enzyme. *Amino Acids* **49**, 415–423.

12 Kumar A, Xu J, Sung B, Kumar S, Yu D, Aggarwal BB & Mehta K (2012) Evidence that GTP-binding domain but not catalytic domain of transglutaminase 2 is essential for epithelial-to-mesenchymal transition in mammary epithelial cells. *Breast Cancer Res* **14**, R4.

13 Lin HY, Kuei CH, Lee HH, Lin CH, Zheng JQ, Chiu HW, Chen CL & Lin YF (2020) The Gαh/phospholipase C-δ1 interaction promotes autophagosome degradation by activating the Akt/mTORC1 pathway in metastatic triple-negative breast cancer. *Aging (Albany NY)* **12**, 13023–13037.

14 Datta S, Antonyak MA & Cerione RA (2006) Importance of Ca(2+)-dependent transamidation activity in the protection afforded by tissue transglutaminase against doxorubicin-induced apoptosis. *Biochemistry* **45**, 13163–13174.

15 Shinde A, Paez JS, Libring S, Hopkins K, Solorio L & Wendt MK (2020) Transglutaminase-2 facilitates extracellular vesicle-mediated establishment of the metastatic niche. *Oncogenesis* **9**, 16–28.

16 Cooper AJ, Sheu KR, Burke JR, Onodera O, Strittmatter WJ, Roses AD & Blass JP (1997) Transglutaminase-catalyzed inactivation of glyceraldehyde 3-phosphate dehydrogenase and alpha-ketoglutarate dehydrogenase complex by polyglutamine domains of pathological length. *Proc Natl Acad Sci USA* **94**, 12604–12609.

17 Iwai K, Shibukawa Y, Yamazaki N & Wada Y (2014) Transglutaminase 2-dependent deamidation of glyceraldehyde-3-phosphate dehydrogenase promotes trophoblastic cell fusion. *J Biol Chem* **289**, 4989–4999.

18 Esposito C & Caputo I (2005) Mammalian transglutaminases. Identification of substrates as a key to physiological function and physiopathological relevance. *FEBS J* **272**, 615–631.

19 Cordella-Miele E, Miele L, Beninati S & Mukherjee AB (1993) Transglutaminase-catalyzed incorporation of polyamines into phospholipase A2. *J Biochem* **113**, 164–173.

20 Currò M, Ferlazzo N, Risitano R, Condello S, Vecchio M, Caccamo D & Ientile R (2014) Transglutaminase 2 and phospholipase a₂ interactions in the inflammatory response in human Thp-1 monocytes. *Amino Acids* **46**, 759–766.

21 Feng JF, Rhee SG & Im MJ (1996) Evidence that phospholipase delta1 is the effector in the Gh (transglutaminase II)-mediated signaling. *J Biol Chem* **271**, 16451–16454.

22 Kim DS, Park KS & Kim SY (2009) Silencing of TGase 2 sensitizes breast cancer cells to apoptosis by regulation of survival factors. *Front Biosci (Landmark Ed)* **14**, 2514–2521.

23 He W, Sun Z & Liu Z (2015) Silencing of TGM2 reverses epithelial to mesenchymal transition and modulates the chemosensitivity of breast cancer to docetaxel. *Exp Ther Med* **10**, 1413–1418.

24 Budillon A, Carbone C & Di Gennaro E (2013) Tissue transglutaminase: a new target to reverse cancer drug resistance. *Amino Acids* **44**, 63–72.

25 Eckert RL (2019) Transglutaminase 2 takes center stage as a cancer cell survival factor and therapy target. *Mol Carcinog* **58**, 837–853.

26 Aguiari G, Crudele F, Taccioli C, Minotti L, Corrà F, Keillor JW, Grassilli S, Cervellati C, Volinia S, Bergamini CM et al. (2022) Dysregulation of transglutaminase type 2 through GATA3 defines aggressiveness and doxorubicin sensitivity in breast cancer. *Int J Biol Sci* **18**, 1–14.

27 Kerr C, Szmacinski H, Fisher ML, Nance B, Lakowicz JR, Akbar A, Keillor JW, Lok Wong T, Godoy-Ruiz R, Toth EA et al. (2017) Transamidase site-targeted agents alter the conformation of the transglutaminase cancer stem cell survival protein to reduce GTP binding activity and cancer stem cell survival. *Oncogene* **36**, 2981–2990.

28 Jambrovics K, Uray IP, Keresztessy Z, Keillor JW, Fésüs L & Balajthy Z (2019) Transglutaminase 2 programs differentiating acute promyelocytic leukemia cells in all-trans retinoic acid treatment to inflammatory stage through NF-κB activation. *Haematologica* **104**, 505–515.

29 Jambrovics K, Uray IP, Keillor JW, Fésüs L & Balajthy Z (2020) Benefits of combined all-trans retinoic acid and arsenic trioxide treatment of acute promyelocytic leukemia cells and further enhancement by inhibition of atypically expressed transglutaminase 2. *Cancers (Basel)* **12**, 648–662.

30 Baillie TA (2016) Targeted covalent inhibitors for drug design. *Angew Chem Int Ed Engl* **55**, 13408–13421.

31 Mader L, Watt SKI, Iyer HR, Nguyen L, Kaur H & Keillor JW (2022) The war on hTG2: warhead optimization in small molecule human tissue transglutaminase inhibitors. *RSC Med Chem* **14**, 277–298.

32 Akbar A, McNeil NMR, Albert MR, Ta V, Adhikary G, Bourgeois K, Eckert RL & Keillor JW (2017) Structure-activity relationships of potent; targeted covalent inhibitors that abolish both the transamidation and GTP binding activities of human tissue transglutaminase. *J Med Chem* **60**, 7910–7927.

33 Bergamini CM, Dondi A, Lanzara V, Squerzanti M, Cervellati C, Montin K, Mischiati C, Tasco G, Collighan R, Griffin M et al. (2010) Thermodynamics of binding of regulatory ligands to tissue transglutaminase. *Amino Acids* **39**, 297–304.

34 Rangaswamy AMM, Navals P, Gates EWJ, Shad S, Watt SKI & Keillor JW (2022) Structure-activity relationships of hydrophobic alkyl acrylamides as tissue transglutaminase inhibitors. *RSC Med Chem* **13**, 413–428.

35 Li C, Li X, Li G, Sun L, Zhang W, Jiang J & Ge Q (2020) Identification of a prognosis-associated signature associated with energy metabolism in triple-negative breast cancer. *Oncol Rep* **44**, 819–837.

36 Fujita M, Imadome K, Somasundaram V, Kawanishi M, Karasawa K & Wink DA (2020) Metabolic characterization of aggressive breast cancer cells exhibiting invasive phenotype: impact of non-cytotoxic doses of 2-DG on diminishing invasiveness. *BMC Cancer* **20**, 929–942.

37 Schmidt JC, Dougherty BV, Beger RD, Jones DP, Schmidt MA & Mattes WB (2021) Metabolomics as a truly translational tool for precision medicine. *Int J Toxicol* **40**, 413–426.

38 Pavlova NN & Thompson CB (2016) The emerging hallmarks of cancer metabolism. *Cell Metab* **23**, 27–47.

39 DeBerardinis RJ & Chandel NS (2016) Fundamentals of cancer metabolism. *Sci Adv* **2**, e1600200.

40 Draguet A, Tagliatti V & Colet JM (2021) Targeting metabolic reprogramming to improve breast cancer treatment: an in vitro evaluation of selected metabolic inhibitors using a metabolomic approach. *Metabolites* **11**, 556–575.

41 Uifălean A, Schneider S, Gierok P, Ionescu C, Iuga CA & Lalk M (2016) The impact of soy isoflavones on MCF-7 and MDA-MB-231 breast cancer cells using a global metabolomic approach. *Int J Mol Sci* **17**, 1443–1460.

42 Costantini S, Guerriero E, Teta R, Capone F, Caso A, Sorice A, Romano G, Ianora A, Ruocco N, Budillon A et al. (2017) Evaluating the effects of an organic extract from the mediterranean sponge geodia cydonium on

human breast cancer cell lines. *Int J Mol Sci* **18**, 2112–2124.

43 Maria RM, Altei WF, Selistre-de-Araujo HS & Colnago LA (2017) Effects of doxorubicin; cisplatin; and tamoxifen on the metabolic profile of human breast cancer MCF-7 cells as determined by 1H high-resolution magic angle spinning nuclear magnetic resonance. *Biochemistry* **56**, 2219–2224.

44 Maria RM, Altei WF, Selistre-de-Arauj HS & Colnago LA (2017) Impact of chemotherapy on metabolic reprogramming: characterization of the metabolic profile of breast cancer MDA-MB-231 cells using 1H HR-MAS NMR spectroscopy. *J Pharm Biomed Anal* **146**, 324–328.

45 Zhou X, Li Z, Wang X, Jiang G, Shan C & Liu S (2020) Metabolomics reveals the effect of valproic acid on MCF-7 and MDA-MB-231 cells. *Xenobiotica* **50**, 252–260.

46 Del Coco L, Majellaro M, Boccarelli A, Cellamare S, Altomare CD & Fanizzi FP (2020) Novel antiproliferative biphenyl nicotinamide: NMR metabolomic study of its effect on the MCF-7 cell in comparison with cisplatin and vinblastine. *Molecules* **25**, 3502–3516.

47 Zhang B, Fu R, Duan Z, Shen S, Zhu C & Fan D (2022) Ginsenoside CK induces apoptosis in triple-negative breast cancer cells by targeting glutamine metabolism. *Biochem Pharmacol* **202**, 115101–115120.

48 Bhute VJ, Ma Y, Bao X & Palecek SP (2016) The poly (ADP-ribose) polymerase inhibitor veliparib and radiation cause significant cell line dependent metabolic changes in breast cancer cells. *Sci Rep* **6**, 36061–36073.

49 Lemma S, Di Pompo G, Porporato PE, Sboarina M, Russell S, Gillies RJ, Baldini N, Sonveaux P & Avnet S (2017) MDA-MB-231 breast cancer cells fuel osteoclast metabolism and activity: a new rationale for the pathogenesis of osteolytic bone metastases. *Biochim Biophys Acta Mol Basis Dis* **1863**, 3254–3264.

50 Lanning NJ, Castle JP, Singh SJ, Leon AN, Tovar EA, Sanghera A, MacKeigan JP, Filipp FV & Graveel CR (2017) Metabolic profiling of triple-negative breast cancer cells reveals metabolic vulnerabilities. *Cancer Metab* **5**, 6–20.

51 Gong Y, Ji P, Yang YS, Xie S, Yu TJ, Xiao Y, Jin ML, Ma D, Guo LW, Pei YC *et al.* (2021) Metabolic-pathway-based subtyping of triple-negative breast cancer reveals potential therapeutic targets. *Cell Metab* **33**, 51–64.

52 Bao L, Hazari S, Mehra S, Kaushal D, Moroz K & Dash S (2012) Increased expression of P-glycoprotein and doxorubicin chemoresistance of metastatic breast cancer is regulated by miR-298. *Am J Pathol* **180**, 2490–2503.

53 Abu Ajaj K, Graeser R & Kratz F (2012) Zosuquidar and an albumin-binding prodrug of zosuquidar reverse multidrug resistance in breast cancer cells of doxorubicin and an albumin-binding prodrug of doxorubicin. *Breast Cancer Res Treat* **134**, 117–129.

54 Verhaar R, Jongenelen CA, Gerard M, Baekelandt V, Van Dam AM, Wilhelmus MM & Drukarch B (2011) Blockade of enzyme activity inhibits tissue transglutaminase-mediated transamidation of α-synuclein in a cellular model of Parkinson's disease. *Neurochem Int* **58**, 785–793.

55 Yamaguchi H & Wang HG (2006) Tissue transglutaminase serves as an inhibitor of apoptosis by cross-linking caspase 3 in thapsigargin-treated cells. *Mol Cell Biol* **26**, 569–579.

56 Malkomes P, Lunger I, Oppermann E, Abou-El-Ardat K, Oellerich T, Günther S, Canbulat C, Bothur S, Schnütgen F, Yu W *et al.* (2021) Transglutaminase 2 promotes tumorigenicity of colon cancer cells by inactivation of the tumor suppressor p53. *Oncogene* **40**, 4352–4367.

57 McNeil NMR, Gates EWJ, Firoozi N, Cundy NJ, Leccese J, Eisinga S, Tyndall JDA, Adhikary G, Eckert RL & Keillor JW (2022) Structure-activity relationships of N-terminal variants of peptidomimetic tissue transglutaminase inhibitors. *Eur J Med Chem* **232**, 114172–114196.

58 Sonkar K, Ayyappan V, Tressler CM, Adelaja O, Cai R, Cheng M & Glunde K (2016) Focus on the glycerophosphocholine pathway in choline phospholipid metabolism of cancer. *NMR Biomed* **32**, e4112–e4174.

59 Mattaini KR, Sullivan MR & Vander Heiden MG (2016) The importance of serine metabolism in cancer. *J Cell Biol* **214**, 249–257.

60 Arike L, Hansson GC & Recktenwald CV (2020) Identifying transglutaminase reaction products via mass spectrometry as exemplified by the MUC2 mucin – pitfalls and traps. *Anal Biochem* **597**, 113668–113673.

61 Ai L, Kim WJ, Demircan B, Dyer LM, Bray KJ, Skehan RR, Massoll NA & Brown KD (2008) The transglutaminase 2 gene (TGM2), a potential molecular marker for chemotherapeutic drug sensitivity, is epigenetically silenced in breast cancer. *Carcinogenesis* **29**, 510–518.

62 Carbone C, Di Gennaro E, Piro G, Milone MR, Pucci B, Caraglia M & Budillon A (2017) Tissue transglutaminase (TG2) is involved in the resistance of cancer cells to the histone deacetylase (HDAC) inhibitor vorinostat. *Amino Acids* **49**, 517–528.

63 Hlaváč V, Václavíková R, Brynychová V, Koževnikovová R, Kopečková K, Vrána D, Gatěk J & Souček P (2020) Role of genetic variation in ABC transporters in breast cancer prognosis and therapy response. *Int J Mol Sci* **21**, 9556–9573.

64 Cundy NJ, Arciszewski J, Gates EWJ, Acton SL, Passley KD, Awoonor-Williams E, Boyd EK, Xu N, Pierson E, Fernandez-Ansieta C *et al.* (2022) Novel

irreversible peptidic inhibitors of transglutaminase 2. *Rsc Med Chem* **14**, 378–385.

65 Podo F, Paris L, Cecchetti S, Spadaro F, Abalsamo L, Ramoni C, Ricci A, Pisanu ME, Sardanelli F, Canese R *et al.* (2016) Activation of phosphatidylcholine-specific phospholipase C in breast and ovarian cancer: impact on MRS-detected choline metabolic profile and perspectives for targeted therapy. *Front Oncol* **6**, 171–179.

66 Muthusamy T, Cordes T, Handzlik MK, You L, Lim EW, Gengatharan J, Pinto AFM, Badur MG, Kolar MJ, Wallace M *et al.* (2020) Serine restriction alters sphingolipid diversity to constrain tumour growth. *Nature* **586**, 790–795.

67 Grinde MT, Skrbo N, Moestue SA, Rødland EA, Borgan E, Kristian A, Sitter B, Bathen TF, Børresen-Dale AL, Mælandsmo GM *et al.* (2014) Interplay of choline metabolites and genes in patient-derived breast cancer xenografts. *Breast Cancer Res* **16**, R5–R21.

68 Kang SK, Yi KS, Kwon NS, Park KH, Kim UH, Baek KJ & Im MJ (2004) Alpha1B-adrenoceptor signaling and cell motility: GTPase function of Gh/transglutaminase 2 inhibits cell migration through interaction with cytoplasmic tail of integrin alpha subunits. *J Biol Chem* **279**, 36593–36600.

69 Iismaa SE, Begg GE & Graham RM (2006) Cross-linking transglutaminases with G protein-coupled receptor signaling. *Sci STKE* **353**, pe34.

70 Huang SP, Liu PY, Kuo CJ, Chen CL, Lee WJ, Tsai YH & Lin YF (2017) The Gαh-PLCδ1 signaling axis drives metastatic progression in triple-negative breast cancer. *J Hematol Oncol* **10**, 114–127.

71 D'Eletto M, Rossin F, Occhigrossi L, Farrace MG, Faccenda D, Desai R, Marchi S, Refolo G, Falasca L, Antonioli M *et al.* (2018) Transglutaminase type 2 regulates ER-mitochondria contact sites by interacting with GRP75. *Cell Rep* **25**, 3573–3581.e4.

72 Malorni W, Farrace MG, Matarrese P, Tinari A, Ciarlo L, Mousavi-Shafaei P, D'Eletto M, Di Giacomo G, Melino G, Palmieri L *et al.* (2009) The adenine nucleotide translocator 1 acts as a type 2 transglutaminase substrate: implications for mitochondrial-dependent apoptosis. *Cell Death Differ* **16**, 1480–1492.

73 Sedano MJ, Ramos EI, Choudhari R, Harrison AL, Subramani R, Lakshmanaswamy R, Zilaie M & Gadad SS (2020) Hypoxanthine phosphoribosyl transferase 1 is upregulated; predicts clinical outcome and controls gene expression in breast cancer. *Cancers (Basel)* **12**, 1522–1535.

74 Chhetri DR (2019) Myo-inositol and its derivatives: their emerging role in the treatment of human diseases. *Front Pharmacol* **10**, 1172–1180.

75 Deng F, Zheng X, Sharma I, Dai Y, Wang Y & Kanwar YS (2021) Regulated cell death in cisplatin-induced AKI: relevance of myo-inositol metabolism. *Am J Physiol Renal Physiol* **320**, F578–F595.

76 Amabile MI, De Luca A, Tripodi D, D'Alberti E, Melcarne R, Imbimbo G, Picconi O, D'Andrea V, Vergine M, Sorrenti S *et al.* (2021) Effects of inositol hexaphosphate and myo-inositol administration in breast cancer patients during adjuvant chemotherapy. *J Pers Med* **11**, 756–771.

77 Comşa Ş, Cîmpean AM & Raica M (2015) The story of MCF-7 breast cancer cell line: 40 years of experience in research. *Anticancer Res* **35**, 3147–3154.

78 Huang Z, Yu P & Tang J (2020) Characterization of triple-negative breast cancer MDA-MB-231 cell spheroid model. *Onco Targets Ther* **13**, 5395–5405.

79 Franzese O, Minotti L, Aguiari G, Corrà F, Cervellati C, Ferrari C, Volinia S, Bergamini CM & Bianchi N (2019) Involvement of non-coding RNAs and transcription factors in the induction of transglutaminase isoforms by ATRA. *Amino Acids* **51**, 1273–1288.

80 Gallo M, Giovati L, Magliani W, Pertinhez TA, Conti S, Ferrari E, Spisni A & Ciociola T (2022) Metabolic plasticity of candida albicans in response to different environmental conditions. *J Fungi (Basel)* **8**, 723–738.

81 Pang Z, Chong J, Zhou G, de Lima Morais DA, Chang L, Barrette M, Gauthier C, Jacques PÉ, Li S & Xia J (2021) MetaboAnalyst 5.0: narrowing the gap between raw spectra and functional insights. *Nucleic Acids Res* **49**, W388–W396.

82 Worley B & Powers R (2013) Multivariate analysis in metabolomics. *Curr Metabolomics* **1**, 92–107.

RIGHTS LINK()